Chapter 8

Dynamic Cardiac Single-Photon Emission Computed Tomography Using Fast Data Acquisition Systems

Grant T. Gullberg, Ronald H. Huesman, Edward V. R. Di Bella, Bryan W. Reutter

Introduction

Currently, myocardial perfusion imaging,[1] particularly with single-photon emission computed tomography (SPECT),[2–19] is the most widely employed noninvasive method for the diagnosis and risk stratification of patients with known or suspected coronary artery disease. The number of scintigraphic perfusion evaluations done in the United States now exceeds 7 million per year. The scintigraphic method provides a practical, noninvasive measure of myocardial perfusion and its hyperemic response to stress, which is the primary parameter directly affected by flow-limiting coronary stenoses and is the common basis of all stress testing for the diagnosis and risk stratification of coronary artery disease.[20–25] There is significant interest in developing methods to compete with myocardial perfusion imaging, yet little is being done to improve the basic method of perfusion scintigraphy. Because no new radiopharmaceuticals (the basis for the method) have been introduced for many years, new methods such as dynamic cardiac SPECT may offer the only potential to improve risk stratification in cases of moderate to mild disease. The use of multidetector SPECT systems is producing results[26–32] that show that dynamic cardiac SPECT imaging of agents such as thallium-201[26,27] or technetium-99m–teboroxime[28–31] can accurately measure perfusion in myocardial tissue. The results also show that dynamic imaging may be a more sensitive measure of ischemia than static imaging of perfusion agents, and that potentially both perfusion and myocardial viability assessments can be obtained during a single imaging session.

Developments in dynamic cardiac SPECT draw heavily on developments in positron emission tomography (PET),[33–52] in particular, the work that has been accomplished in modeling the kinetics of perfusion of rubidium-82,[33–39] N-13-ammonia,[33,40–47] and $H_2{}^{15}O$.[48–52] Many of the data analysis challenges faced in dynamic cardiac PET are also encountered in dynamic cardiac SPECT, but the problems are exacerbated in SPECT because of more complicated imaging physics related to attenuation, poor statistics, poor spatial resolution, and poor timing resolution that occur as a result of the mechanical rotation of the detector. Still, many of the solutions implemented in PET are applicable to SPECT. For example, there is the problem of partial volume effects. This can affect tissue contamination of the blood input function obtained from a time-activity curve generated from a region of interest (ROI) in the left ventricular cavity.[53] In PET, researchers have investigated the use of $C^{15}O$ (which remains intravascular due to hemoglobin binding) to correct for spillover from tissue to blood.[48–51] In these works it is suggested that an intravascular tracer, such as radiolabeled albumin or red blood cells, be used to correct for tissue-to-blood contamination in dynamic SPECT. It also may be possi-

ble to include the spillover as an unknown fraction in the model.[54] A second problem is the partial volume effect that alters the bias of the estimated parameters. Based on the work of Hutchins and colleagues,[55] we were able to develop a strategy for sampling the myocardium in order to minimize the partial volume effect in SPECT (see Chapter 3).[56] An intravascular tracer can also eliminate partial volume effects in SPECT,[57] much as $C^{15}O$ has been used to estimate tissue fraction and correct for partial volume effects in PET.[58] A third problem is the retention of the tracer in the blood.[53,59] Work in PET, in which measurements of metabolites of N-13-ammonia in the blood[44,45] were used to obtain more accurate blood input functions, suggests that these techniques could be applied to measuring the retention of Tc-99m–teboroxime in the blood. A fourth problem is the effect that results from input function shape, timing resolution of the SPECT system, and intervals between samples on the bias and precision of the kinetic parameters. In PET, this set of problems has been investigated in some detail[60,61] and has been addressed in dynamic SPECT as well.[62,63] Another problem in SPECT is that the agent distribution changes during rotational acquisition.[62,64,65] This has motivated us to develop methods that estimate kinetic parameters directly from measured projections.[66,67,67A]

It was originally hypothesized, based on work performed on a ring-detector SPECT system,[68] that dynamic SPECT imaging and kinetic modeling of the rapid washin and washout kinetics of Tc-99m–teboroxime could be used to estimate myocardial blood flow. Original work with multidetector (three detectors) systems concentrated on relatively long acquisition times to obtain estimates of the washout of Tc-99m–teboroxime from the myocardium. Nakajima and colleagues[69] were the first to use a commercial three-detector SPECT system to obtain 360-degree tomographic acquisitions every 1 minute by using continuous rotation for a period of 15 minutes. Dynamic reconstructed data of the Tc-99m–teboroxime washout phase from the heart were obtained and fit to a bi-exponential function to measure reperfusion after an ischemic insult. A similar protocol was used by Chua and colleagues[70] to obtain a relative measure of the washout kinetics. The original work of Budinger and colleagues[71] demonstrated that a three-detector system could acquire dynamic cardiac SPECT data of 360 degrees of angular sampling every 5 seconds, which could then be used to measure the kinetics of Tc-99m–pertechnetate. Our research[27,28,29,31,72,73] built on this to demonstrate that 5- and 10-second tomographic acquisitions could be acquired and used to estimate both the washin and washout of Tc-99m–teboroxime in canines, using kinetic compartment modeling techniques. This was later demonstrated to be possible in human subjects.[27,32,72,73] Another application of recent interest is using dynamic cardiac SPECT to measure the perfusion of Tl-201 and its distribution volume in the heart. Iida and Eberl[24,74] published early on results obtained from canine studies in which good correlation of flow values with microspheres was demonstrated. More recently, we have obtained similar results.[27,73] It is hypothesized that the distribution volume of Tl-201 or Tc-99m–teboroxime in cardiac tissue is a good indicator of tissue viability. Preliminary results obtained in our laboratory are presented in this chapter.

The standard single gamma camera configuration for SPECT has been supplanted at many institutions by dual- or triple-detector systems, with dual-detector systems being most prevalent. However, single-detector systems are still most common in clinic inventory given the significant numbers of them acquired by institutions over the last 15 years. Various four-sided detector systems have been designed for dynamic SPECT of the brain, but not of the heart. The Kuhl and Edwards[75] device developed 30 years ago for Tc-99m imaging was followed in 1978 by the Xe-131 imaging system,[76] which is capable of 5-second sampling, and more recently by the four gamma camera system of Kimura and colleagues.[77] Only two ring SPECT systems have been proposed for cardiac imaging: the Shimadzu whole-body system[78] and the cardiac FastSPECT system[79]; but they still are only conceptual designs. Currently, most ring systems are dedicated brain systems[80–84] and are housed in research institutions. The brain FastSPECT system developed at the University of Arizona consists of a hemispherical multiple-pinhole coded aperture and 20 small (100 × 100 mm crystal area) digital gamma cameras, which allow multiple simultaneous cone-beam views, thus making feasible the acquisition of volumetric dynamic images without any detector motion.[84] This group has reported dynamic tomographic acquisitions with a sampling interval of 2 seconds. These nonrotating detector systems are ideal for dynamic SPECT. However, rotating three-detector systems have been shown to provide adequate temporal resolution. With new techniques for data analysis, single-detector SPECT systems may also produce positive results.

New multigamma camera systems have the mechanical stability and control hardware to allow 360-degree acquisition of data in 5 to 10 seconds. These systems allow volumetric imaging, but need not sample at rates less than 5 seconds because the statistical data available are still insufficient, even with injections of 1110 MBq (30 mCi) of Tc-99m to warrant more rapid sampling. The need to match the shape of the input function to the frequency response of the myocardium with high statistics during critical phases (fast variation) of time-activity curves of the dynamic system makes it difficult to select both an optimal input function shape and an

acquisition interval long enough to maximize statistics, yet short enough to capture the timing resolution necessary to accurately reproduce the time variation in the time-activity curves. One study[62] has shown that longer acquisition intervals (10, 20, 40 seconds) result in the most accurate estimates of kinetic parameters when kinetics are fast, such as during stress. At rest, with low statistics, a bolus infusion always provides optimal estimates of kinetic parameters. The smallest amount of bias is observed when utilizing a 10-second acquisition and the smallest amount of variance is seen when a 20-second acquisition is used. When the count rates are doubled, longer infusions and shorter acquisitions provide more accurate estimates of kinetic parameters during a resting state. When kinetics are increased during stress, longer acquisitions result in better estimates. This indicates that better signal-to-noise ratios are required in order to estimate fast kinetics. The major advantage of multiple camera systems is the improvement in sensitivity that results when more detector material surrounds the patient. Through the use of four-detector banks rather than one-detector banks, the relative sensitivity advantage of PET over SPECT is reduced from 80 to 20 times for a 7-mm resolution. Another advantage is that multiple detectors reduce the angular range of motion necessary to acquire a complete data set. Thus, only a 90-degree rotation is needed for a four-detector system and 120 degrees is needed for a three-detector system. The disadvantage is that multiple camera systems are expensive, and fast rotations are not available on all systems.

In this chapter some of the more recent developments in dynamic cardiac SPECT with fast data acquisition are summarized. First, compartment modeling techniques are discussed. Examples of utilizing a one-compartment model for dynamic cardiac SPECT are given. Then, methods for estimating the kinetic parameters from dynamic reconstructions are presented. Following that an automatic technique for estimating parametric images at the same resolution of present-day cardiac SPECT images is presented. This is accomplished automatically, whereby the input function is determined using factor analysis of dynamic structures (FADS). Finally, results of canine and patient studies are presented. Specifically, it is shown how dynamic SPECT may potentially play a significant role in diagnosing cardiac perfusion, cardiac viability, and myocardial coronary flow reserve (CFR).

Principles of Tracer Kinetic Modeling (see Chapter 1)

Tracer kinetic modeling is used in several areas of biologic research to follow dynamic processes of blood flow, tissue perfusion, transport, metabolism, and receptor binding.[85–94] The principles are based on the early work of Fick,[85] Stewart,[86,87] Hamilton and colleagues,[88] and later that of Kety and Schmidt.[89] It was Zierler, though in the 1950s[90] and 1960s,[91] who developed equations for many of these original principles. He formulated general equations for estimating flow using tracers for both the inflow injection/outflow technique and the inflow injection/residue detection technique.[94] The latter applies when external detection is used to measure the time sequence of tracer content in an organ, like that which is done with dynamic PET and dynamic SPECT.

PRINCIPLE OF COMPARTMENTALIZATION

The modeling of tracer kinetics relies on the principle of indicator dilution, whereby models are developed that compartmentalize the dilution of a measurable tracer that is introduced in the biological system to be studied to follow a physiologic or biochemical process of a particular biochemical substance.[93] An appropriate tracer must be chosen to ensure that it follows the dynamic process of interest, is measurable, and does not perturb the process being measured. Upon introduction, the tracer distributes throughout the sample. Measurements of the tracer are taken as a function of time.

The compartmentalization is based on a priori knowledge of structural or configurational information about the process or the organ system. Based on this information a compartment model is developed that gives a mathematical description of the pathways and dynamic behavior of the tracer in the biological tissue of interest. The model is represented by a number of compartments (volumes where the tracer is uniformly distributed[93]) linked together by arrows indicating transport between the various compartments. The amount of tracer leaving a compartment is usually assumed to be proportional to the total amount in the compartment. The constant of proportionality (the rate constant) has the unit of inverse time and denotes the fraction of the total tracer that will leave the compartment per unit time. The kinetics between compartments is described by a system of differential equations.

For example, suppose you have a blood compartment with concentration $B(t)$ and an extravascular compartment with concentration $C_2(t)$. The rate equation for the extravascular space is

$$\frac{d}{dt}C_2(t) = -\frac{P_{12}S}{V_2}C_2(t) + \frac{P_{21}S}{V_2}B(t) \qquad (1)$$

where V_2 is the volume of the extravascular compartment, P_{12} and P_{21} (in units of cm/min) are the permeability coefficients for flux out of and into the capillary, respectively, and S (cm^2) is the surface area of the capillary in the sampled voxel. Setting $k_{21} = (P_{21}S)/V_2$ and

$k_{12} = (P_{12}S)/V_2$, the rate constants in and out of the extravascular compartment are in units of volume per minute per extravascular volume (V_2). Substituting k_{21} and k_{12} into Eq. 1, the differential equation describing the exchange between the intravascular and extravascular compartments can be rewritten as

$$\frac{d}{dt}C_2(t) = -k_{12}C_2(t) + k_{21}B(t) \tag{2}$$

where the rate of change in and out of the extravascular compartment is proportional to the concentration in the blood and the concentration in the extravascular compartment, respectively.

The amount of tracer in a volume of tissue can deviate significantly in value from the chemical concentration in individual spaces if the tracer does not distribute uniformly within all the spaces in the tissue. Thus, the distribution volume V_d is defined as the fractional space of volume V_2 that a tracer would occupy in the tissue extravascular space with the same concentration as in the blood[93]:

$$V_d = \frac{(amount\ of\ tracer/mL\ of\ tissue)}{(amount\ of\ tracer/mL\ of\ blood)}. \tag{3}$$

If we assume equilibrium, we can set Eq. 2 to zero, which implies that $k_{21}B(\infty) = k_{12}C_2(\infty)$ or the distribution volume $V_d = C_2(\infty)/B(\infty) = k_{21}/k_{12}$. The definition of the "partition coefficient" is precisely the ratio of the tracer concentration in the tissue to that in the blood at equilibrium. Thus, the distribution volume and partition coefficient have identical value, but different conceptual meanings. The term "partition coefficient" implies that the tracer can distribute throughout the entire tissue space, but the capillary wall forms a partition such that the tracer concentration on the two sides need not be equal. Whereas, the distribution volume implies that there is some space within the volume in which the tracer can distribute. In reality, a tracer does not distribute uniformly throughout the entire tissue space, nor does it have the same concentration in tissue as it has in blood. Therefore, strictly speaking, one should think of the distribution volume or "partition coefficient" only in terms of the definition given in Eq. 3.

COMPARTMENT MODELING OF CARDIAC PERFUSION

For the perfusion model presented in this chapter that can be used to follow the dynamics of either Tl-201 or Tc-99m–teboroxime, it is assumed that $B(t)$ is known, either by sampling the image-derived reconstruction or by measuring plasma samples (Fig. 8.1). In this case we have a one-compartment model (Fig. 8.2) instead of a two-compartment model since the kinetics of the blood compartment are known from an independent measurement. Thus, the differential equation in Eq. 2 completely describes the kinetics of the model. It is assumed that the blood concentration measured in the left ventricular cavity represents the blood concentration of the particular radiopharmaceutical that is available to the myocardium.

Each data point from the blood and tissue time-activity curves represents an accumulation of counts from the radioactive emissions of the radioisotope over the acquisition time Δt. The accumulation of counts in the tissue is modeled as

$$A_T(t_k) = (1 - f_v)\int_{t_k-\Delta t}^{t_k} C_2(t)dt + f_v\int_{t_k-\Delta t}^{t_k} B(t)dt \tag{4}$$

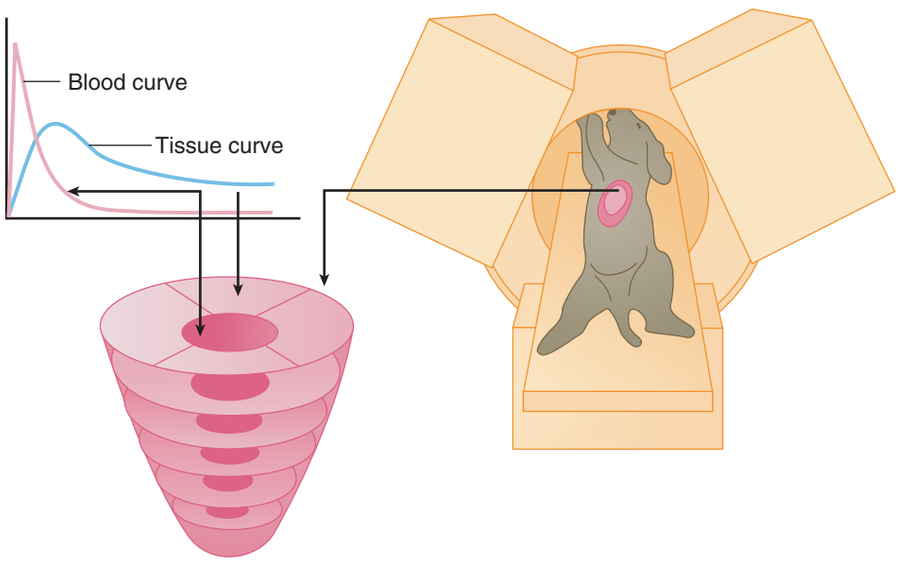

Figure 8.1 Dynamic cardiac SPECT. Dynamic cardiac SPECT is performed by using rapidly rotating gamma cameras to obtain projection measurements, which are used to reconstruct time-activity curves for a blood region of interest and tissue regions of interest. Compartment model parameters are estimated by fitting the time-activity curves to a mathematical model.

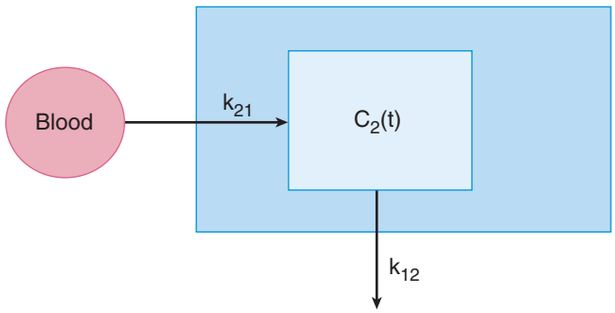

Figure 8.2 One-compartment model for technetium-99m–teboroxime. The rate constants k_{21} and k_{12} are given in (mL/min)/mL of extravascular space.

where A_T is the model of the measured myocardial tissue activity concentration acquired between the time $t_k - \Delta t$ and t_k in the ROI, f_v is the vascular fraction of blood in the tissue, Δt is the acquisition time of the tomographic data set, $B(t)$ is the measured activity concentration from the blood compartment at time t, $C_2(t)$ is the activity concentration from the extravascular compartment at time t, and $(1 - f_v)$ is the fractional volume of the extravascular space. The blood activity concentration $B(t)$ is measured using an ROI drawn inside the left intraventricular cavity.

The activity concentration $C_2(t)$ from the extravascular compartment is given by the first-order ordinary differential equation in Eq. 2, which describes the kinetic exchange between the blood and the extravascular space for the compartment model shown in Figure 8.2. If everything is zero at $t = 0$, the solution to the differential equation in Eq. 2 is

$$C_2(t) = k_{21}\int_0^t e^{-k_{12}(t-\tau)}B(\tau)d\tau. \qquad (5)$$

The parameters k_{21} and k_{12} are the washin and washout rate constants of the radiopharmaceutical, respectively. The units of k_{21} and k_{12} are (mL/min)/(milliliters of extravascular space), but the units of k_{21} and k_{12} are commonly stated simply as min^{-1}.

The one-compartment model shown in Figure 8.2 adheres to the following four assumptions: (1) the time-activity curve of the blood compartment can be measured independently of the extravascular compartment of the myocardial tissue, (2) all myocardial tissue regions exchange with the same blood time-activity curve, (3) the distribution of the tracer is homogeneous throughout the ROI, and (4) the tissue ROI contains only regions from the blood and extravascular compartments. In dynamic cardiac SPECT the kinetic parameters are estimated for multiple three-dimensional regions in the left ventricular myocardium. The vector $\theta = (f_v, k_{21}, k_{12})$ is used to denote the kinetic parameters, where f_v, k_{21}, and k_{12} are vectors with components f_v^s, k_{21}^s, and k_{12}^s denoting each tissue region s.

Comments and references. There is one point of caution. Even though Tc-99m–teboroxime is highly extracted on the first pass, the work of Rumsey and colleagues[95] indicates that extraction from subsequent passes may be affected by the binding of Tc-99m–teboroxime to blood cells and plasma proteins. The effect of this on the bias of the model estimates has been reported by Smith and Gullberg.[53] Here it is assumed that the percentage of binding is small. Also, it has been proposed that a two-compartment model is more appropriate for Tl-201 kinetics and that it is important to sample blood void of red blood cells to obtain an accurate input function.[74] We also direct the reader to an earlier chapter[96] for examples of application of two- and three-compartment models to measure cardiac glucose and fatty acid metabolism.

Estimation of Kinetic Parameters with Noisy Input Function

The purpose of parameter estimation in dynamic cardiac SPECT is to extract mathematically physiological information about cardiac function from dynamically measured data. In this chapter the estimation of the kinetic parameters is considered to be a two-step process that differs from the one-step approach of estimating them directly from the projections.[66,67] Data are collected using a rotating gamma camera (or cameras; see Fig. 8.1). For some SPECT systems tomographic projection sets of 120 projection angles can be acquired in as little as 5 seconds.[29] The projection data are reconstructed to obtain a time sequence of three-dimensional reconstructions of the radiolabeled tracer. For the perfusion model in the section on Compartment Modeling of Cardiac Perfusion, it was assumed that a blood input function can be determined. This function is noisy because it is obtained either from the reconstructed images by drawing an ROI in either the atrium or the left ventricular cavity, or by withdrawing blood and counting the blood samples in a well counter. A set of ROIs for the myocardium is usually defined on the summed image and time-activity curves are generated for each myocardial tissue region. The time-activity curves of the blood input and myocardial tissue (see Fig. 8.1) are then fit to a compartment model that represents the tracer kinetics by using a fitting routine such as region of interest fitting (RFIT).[97] Some of the details[98] of this process are given in the following subsections.

ESTIMATION OF RECONSTRUCTED TRANSAXIAL IMAGES

Iterative reconstruction algorithms are used to reconstruct the dynamically acquired projections in order to model the attenuation, geometric point response, and scatter in the projection equations so their effects can be corrected. Iterative maximum likelihood expectation maximization (ML-EM),[99] ordered subset expectation maximization (OS-EM),[100] and maximum a posteriori (MAP) expectation maximization (MAP-EM) algorithms[101] are used to obtain reconstructions from dynamic tomographic data sets.

The MAP reconstruction of the image f from projection measurements g is obtained by maximizing the log of the a posteriori probability function

$$\Gamma(f) = \log(p(g|f)) - \frac{1}{2}\gamma^2 f^T R f \tag{6}$$

where

$$\log(p(g|f)) = \sum_m \left(g_m \log\left(\sum_{i=1}^{N} F_{mi} f_i \right) - \sum_{i=1}^{N} F_{mi} f_i - \log(g_m!) \right) \tag{7}$$

and $-(\gamma^2/2) f^T R f$ is the log of the prior term with parameter γ and symmetric positive definite matrix R. At the solution we obtain an expression for noise propagation using the fixed-point analysis $\varepsilon = En$ where n is a vector of additive projection noise, ε is a vector of additive image noise, and

$$E = \left[F^T \Lambda_g^{-1} F + \gamma^2 R \right]^{-1} F^T \Lambda_g^{-1}. \tag{8}$$

The matrix F is the projection matrix and the matrix Λ_g is a diagonal matrix of mean projection data values along the diagonal. The covariance matrix for the reconstructed values at the solution is given by the approximation[102] $\text{cov}(f) \approx E\,\text{cov}(n)E^T$. We usually assume that $\text{cov}(n) = \Lambda_g$. The expression in Eq. 8 leads to the fixed-point solution for the covariance matrix of the MAP reconstruction.

Figure 8.3 shows the results for the weighted least squares reconstructions and the iterative MAP reconstructions for simulated data with and without noise. It is obvious from the results that the MAP reconstruction considerably suppresses the noise. Also, the MAP reconstruction without noise shows undershoots around the edge of the myocardium due to the formulation of the prior as a 3×3 smoothing kernel.

ESTIMATION OF KINETIC PARAMETERS

The second step in the estimation procedure is to estimate compartment model parameters from time-activity curves generated from the dynamic reconstructions. The projections are reconstructed for each complete dynamic projection data set, creating a set of three-dimensional reconstructions sequenced in time. Blood and tissue time-activity curves are generated from the sequence of dynamic reconstructions. The reconstruction process correlates errors in the blood and tissue measurements. Variances of and covariances between points on blood and tissue time-activity curves are calculated with use of Eq. 8.[103] As shown in the section on Principles of Tracer Kinetic Modeling, the compartment model depends on a blood input function. This function is noisy (has statistical fluctuations) because it is known only from its measurements of the dynamic reconstructions. The kinetic parameters are estimated for each ROI by fitting the measured tissue data to a model of the dynamic emission tomographic reconstructions using a noisy input function.[98]

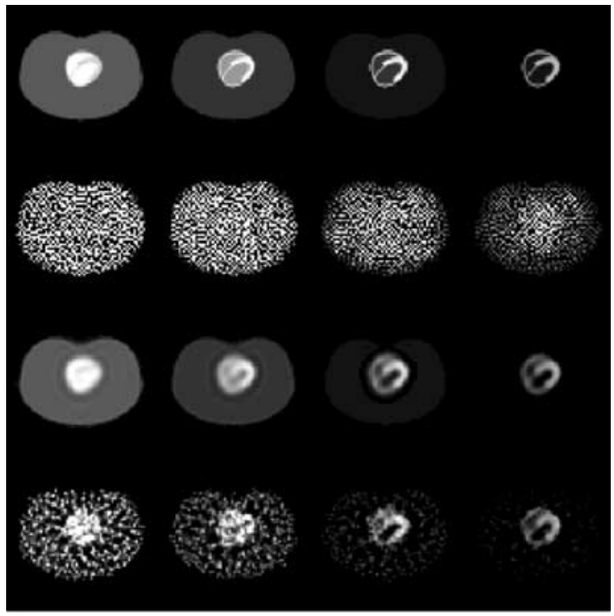

Figure 8.3 Sampled reconstructed time sequences for simulated MCAT phantom data. The *first row* is weighted least squares. The *second row* is weighted least squares with noise. The *third row* is MAP reconstruction (100 iterations) without noise. The *fourth row* is MAP reconstruction with noise.

Figure 8.4 shows the variance time sequences for the blood and myocardial ROIs and the time sequence for the negative of the covariance between blood and myocardial ROIs. The discontinuities in the curves are the result of changes in the length of the acquisition interval.

Figure 8.5 gives the results of the fit for the time sequences generated from the MAP reconstruction with noise. The background curve (lowest curve) illustrates that the reconstructed values match well with the simulated data. The background region is all pixels in the tissue cross section excluding the central myocardial

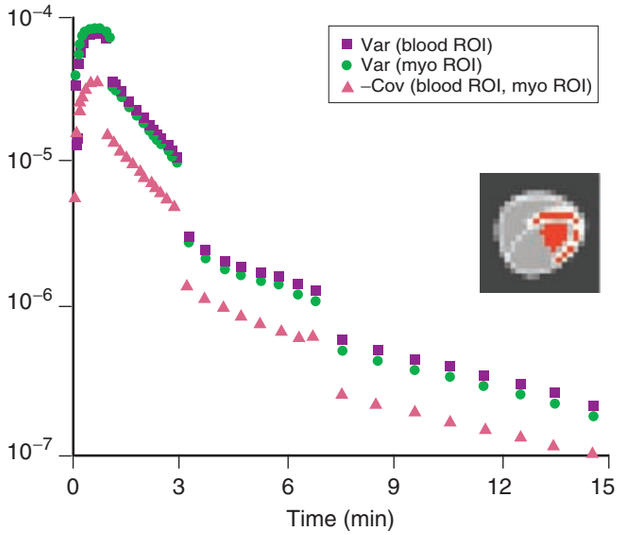

Figure 8.4 Variance time sequences for the blood and myocardial ROIs shown in inset figure on the right and time sequence for the covariance between blood and myocardial ROIs. The discontinuities in the curves are the result of changes in the acquisition interval. Note, the negative of the covariance is shown in this plot.

blood and tissue regions. Regularization causes a blurring of blood into the tissue. This is reflected in the increase in f_v from the simulated value of 0.150. The blood fraction increased, thus the tissue fraction has decreased, which is reflected by a decrease in the myocardium curve in Figure 8.5. Notice also because of the negative correlation between blood and tissue regions, a positive noise increase above the fitted curve corresponds to a negative variation in the tissue curve and visa versa.

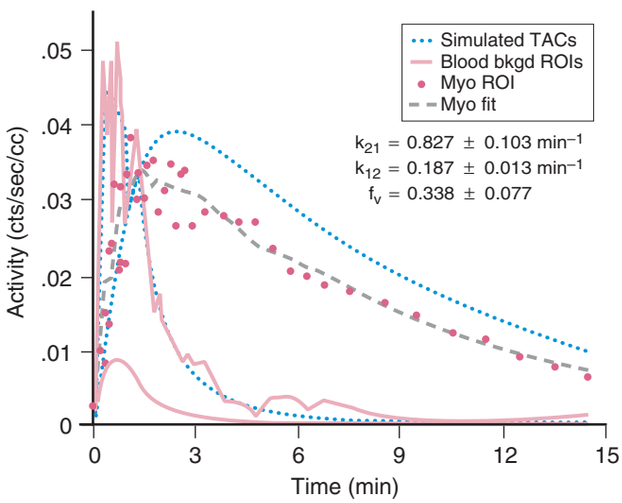

Figure 8.5 Fit for the time sequences generated from the Bayesian reconstruction with noise. The simulated values were k_{21} = 0.824 min^{-1} for the washin rate constant, k_{12} = 0.150 min^{-1} for the washout rate constant, and f_v = 0.150 for the blood fraction.

Comments and references. If a rotating gamma camera SPECT system is used to measure an injected tracer, then the detectors (see Fig. 8.1) must rotate fast enough for the reconstruction to adequately measure the concentration as a function of time. However, if during the acquisition of one tomographic data set the distribution of the tracer in the myocardium changes, then there is an impetus to develop methods that can be used to estimate the model parameters directly from the projections.[66,67] In the data analysis, the blood is usually measured directly from image-derived data (the reconstructions), but it may be obtained either from samples of drawn blood or from intra-arterial catheters shunted for external counting. There are also other possibilities for defining the input function.[96,104,105] Parameter estimation is a branch of mathematics and statistics[106–108] that involves the development of methods that make efficient use of data in the process of estimating parameters of mathematical models. Also, the process of parameter estimation involves the interplay between experimental design, model specification, and techniques of data collection.[109] Careful statistical analysis and hypothesis testing of the results provide a feedback mechanism whereby the model, the data collection protocol, and the parameter estimation process can be evaluated and modified.

Estimation of Parametric Images

In this section a method is developed for better representation of dynamic data that will allow easier and better interpretation of the results. The method involves calculation of kinetic parameters for every pixel in the image, followed by the creation of parametric images, which are derived from a dynamic SPECT study. The parametric representation is based on the one-compartment kinetic model of teboroxime dynamics in the myocardium. Kinetic parameters are calculated for each pixel by using a time-activity curve for each pixel. The parameter values are then mapped to colors or gray levels and displayed as images. Parametric imaging has been used previously in cardiac studies to describe thallium kinetics.[74] The method was developed with the goal of automatically creating images of kinetic parameters, as is presently done with SPECT images, which show better contrast between infarcts and normal tissue and less liver contamination of the inferior left ventricular wall.

ESTIMATING THE INPUT FUNCTION USING FACTOR ANALYSIS

One important aspect of creating parametric images is using the correct input function. It is expected that the time-activity curves for each pixel are extremely noisy,

and we found that in order for the method to work a blood input function had to be smoothed. In the case where there is a noisy input function and noisy data the optimization process may not converge to a solution. A penalized least squares factor analysis of dynamic structures (PLS-FADS) method[110] is used to find the input function. The factor analysis method gives input function curves that are smoother than curves obtained by ROI measurement methods applied to a series of dynamic images.

In the factor model of dynamic data it is assumed that activity in each pixel is a linear combination of factors F with the coefficients of the linear combination defined in matrix C. Using this assumption, the dynamic data A can be written as $A = CF + \varepsilon$, with ε being an error in A. The size of A is $N \times M$, where N is the number of pixels in the image and M is the number of dynamic images. The matrix of factors F is $P \times M$ and the matrix of the factor coefficients C is $N \times P$, with P being the number of factors. Put simply, it is assumed that the image is built from structures that have the same temporal behaviors. In cardiac imaging such structures are the myocardium, blood pool, and liver.

A formidable problem in dynamic cardiac SPECT is the extraction of consistent blood time-activity curves that are not contaminated by tissue data. The use of a factor analysis for dynamic structures (FADS) approach offers improvement over manual ROI selection in extracting blood time-activity curves from sequences of dynamic SPECT reconstructions. If C and F are to be physically meaningful, they must be nonnegative.

However, one major drawback of FADS is that the solution is not unique when only negativity penalties are used to determine factors and factor coefficients. A new method to correct for ambiguous FADS solutions was developed that penalizes multiple components in the images of the factor coefficients.[110]

ESTIMATING PARAMETRIC IMAGES

Parametric images of the heart based on a one-compartment model can be generated to produce images of blood fraction, washin (k_{21}), and washout (k_{12}) parameters for each pixel in the image. In this model the intensity in the pixel i, $A_T^i(t_k)$ is dependent on the known input blood function $B(t)$ and kinetic parameters k_{21}^i and k_{12}^i by Eqs. 4 and 5 where f_v^i is a fraction of the blood input in a given pixel i. For each pixel in the image, kinetic parameters are found using RFIT.[97] A three-dimensional 27-pixel smoothing kernel is then used to smooth each parametric image. The blood input function can be obtained from the dynamic series by using the PLS-FADS method.[110]

IMPROVED LESION CONTRAST AND REDUCED LIVER INTERFERENCE

Here the application of the method is presented to show that by using parametric representation of the data, the contrast between the defects and normal myocardium in parametric images is improved, and the results are more quantitative in comparison to images that are simple sums of reconstructed images.

The PRISM 3000XP (Picker/Phillips) was used to acquire data for the patient study. A transmission scan was first performed using a Gd-153 line source and fan beam collimators with a 65-cm focal length. The emission acquisition was performed using parallel collimators. The patient was injected with a constant 20-second bolus of 17.8 mCi of Tc-99m–teboroxime. The emission acquisition was begun immediately, acquiring 120 projections over 360 degrees every 10 seconds for a total imaging time of 15 minutes. A total of 90 sets of tomographic data were then reconstructed using 25 iterations of the OS-EM algorithm[99] (4 iterations, subset size 4) with geometric point response correction and attenuation correction utilizing the attenuation maps acquired during the transmission scan. Parametric images of the heart were generated using the optimization process described in the section Estimating Parametric Images.

Figure 8.6 shows parametric and summed images (summed between 2 and 15 minutes) of the heart for the patient study. It can clearly be seen that the contrast

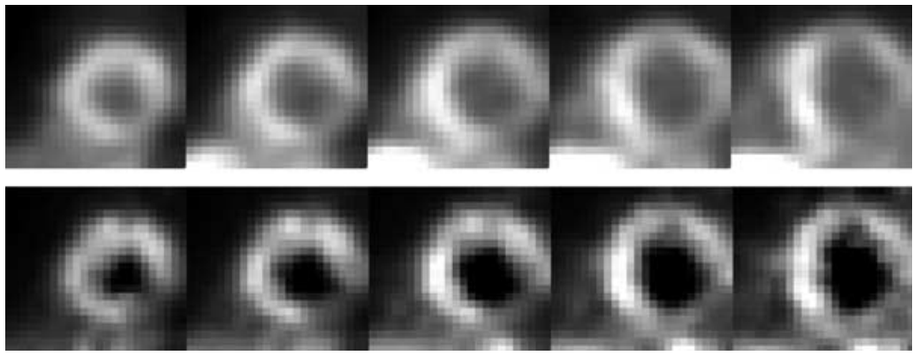

Figure 8.6 Patient parametric images of the heart. The *top row* is short-axis views of images summed between 2 and 15 min of the study. The *bottom row* is parametric images of k_{21}. The gray window level is adjusted to maximum for each image.

between the defects and normal tissue is improved: 0.42 for parametric and 0.60 for summed, for the large inferiolateral defect and 0.65 and 0.67, respectively, for the smaller anterior basal defect. There is much less interference from the liver in the parametric images (bottom row) compared to the liver interference in the summed image (top row). The method tends to increase the contrast between defects and normal myocardial tissue in abnormal hearts and reduce the overlap between the liver and the inferior wall of the left ventricle. With the liver activity removed, the image provides additional information that may be very useful when imaging patients whose liver overlaps the inferior heart wall. More work is needed to determine the degree to which the method can introduce artifacts.

The significant increase in contrast in parametric images of the myocardium (in comparison to the summed images), without any loss in image quality or resolution, suggests that parametric representation of the dynamic data is better for enabling diagnosis of myocardial infarctions. The other aspect of this work is that the volume of distribution (Eq. 3) for infarcted myocardium was smaller than for normal tissue. This could mean that the washin and washout kinetic parameters are related differently to blood flow. That would be a bit surprising because it can be assumed that washin and washout parameters would be in linear relation to the blood flow because of the diffusive nature of teboroxime transport. If this is the case the volume of distribution should be independent of the blood flow. The lower calculated value in the infarcted myocardium may also be the effect of teboroxime binding to the red blood cells, as well as unavailability of the bound teboroxime for the extraction. This hypothesis must be studied more closely.

In SPECT images of patients with their livers positioned close to the heart, the liver may appear to overlap the inferior wall of the heart, making the diagnosis of problems within the inferior wall difficult or impossible. A very important advantage of using parametric images is that the liver interference is reduced. Liver interference is the main drawback of using Tc-99m–teboroxime to image the myocardium. Because the washin of the pharmaceutical into the liver is slower than for the myocardium, this can be used to an advantage even if the integral uptake in the liver is many times higher than it is in the myocardium. This can be seen in the experimental studies presented in this work. As demonstrated, the influence of the liver contamination is greatly diminished if parametric representation of the dynamic data is used.

Comments and references. There are several references to previous work using FADS to analyze dynamic data. The work of Eberl[74] is particularly noteworthy. We developed FADS related to various SPECT applications.[110–113] In one particular study we showed that FADS is useful for reducing liver interference in cardiac studies with Tc-99m–teboroxime.[113] Wu and colleagues[112] were able to extract input functions from dynamic PET studies by using a factor analysis approach and showed that the results correlated highly with ROI measurements. Recently, we also investigated the use of clustering to generate parametric images.[73]

Estimation of Kinetic Parameters in Canine and Patient Studies

The aim of nuclear cardiology is to be able to define perfusion, viability, and ventricular function from a single study.[114] For several years SPECT has been applied to static imaging of the heart utilizing perfusion agents such as Tl-201 and Tc-99m–sestamibi. These, along with newer agents such as tetrofosmin, are now routinely used throughout the world. Teboroxime was approved at the same time as sestamibi, but has not had widespread use for static imaging because of its rather unique pharmacokinetic properties. Paradoxically, there has been very little, if any, activity in the development of new perfusion agents.[114] However, new imaging techniques such as dynamic SPECT are being studied in effort to harness more information from these imaging agents, in particular to effectively image agents with extremely fast kinetic properties and demonstrate their usefulness as clinically relevant procedures.

Recent imaging studies in animals[27–29,31,72,73,96] and patients,[27,32,73] utilizing single- and multidetector SPECT systems, have shown that dynamic cardiac SPECT imaging can measure perfusion in myocardial tissue and may be a more sensitive measure of ischemia than static imaging with perfusion agents. Canine studies have demonstrated that Tc-99m–teboroxime has the potential to quantitatively measure myocardial perfusion.[28,29] We demonstrated that the washin parameter has higher correlations with microsphere measured myocardial perfusion at baseline and with vasodilatation than it does with the washout parameter.[29] In this work we were also able to evaluate the importance of attenuation correction in quantifying kinetic model parameters.[28] We also found that the washin parameter of Tc-99m–teboroxime and the static uptake of Tl-201 both correlated with flow, but the washin parameter of Tc-99m–teboroxime provided greater contrast than the Tl-201 uptake.[31] We compared static versus dynamic myocardial perfusion SPECT with teboroxime in canines using microsphere-derived flow values as the gold standard and showed that the washin rate parameter correlated better with flow than static image intensity in six of seven animal studies.[72] We also demonstrated that dynamic kinetic parameters of Tl-

201 provided higher defect contrast, which was more accurate than the static occluded-to-normal ratios.[27] Using clustering to generate parametric images, we also have been able to show that parametric images of dynamic Tc-99m–teboroxime and dynamic Tl-201 provide better lesion contrast than static images of uptake.[73] In addition, our work includes experimental comparison of the kinetics of Tc-99m–teboroxime, Tl-201, F-18-FDG, and I-123-IPPA using dynamic cardiac SPECT.[96] Recently, we studied the effectiveness of dynamic cardiac SPECT for measuring viability. Similar observations are emerging as more studies using dynamic cardiac SPECT are performed on patients.[27,32,73]

Here, results are presented of canine and patient studies evaluating the usefulness of dynamic cardiac SPECT in the kinetic analysis of Tl-201 and Tc-99m–teboroxime. Dynamic imaging provides physiological parameters of myocardial tissue and is able to utilize tracers with short biological half lives, such as Tc-99m–teboroxime. Dynamic imaging may also provide more versatility for imaging agents such as Tl-201, which previously have only been used for static imaging of cardiac perfusion. It may also be useful for imaging of tracers with fast physiologic turnover, such as Tc-99m–teboroxime. In the following section we discuss estimation of cardiac perfusion, cardiac viability, and cardiac reserve. It is our hypothesis that kinetic parameters obtained from dynamic imaging provide better contrast in perfusion imaging, can provide information about cardiac perfusion and viability in a single study, and in a stress-rest-stress study can quantify coronary reserve.

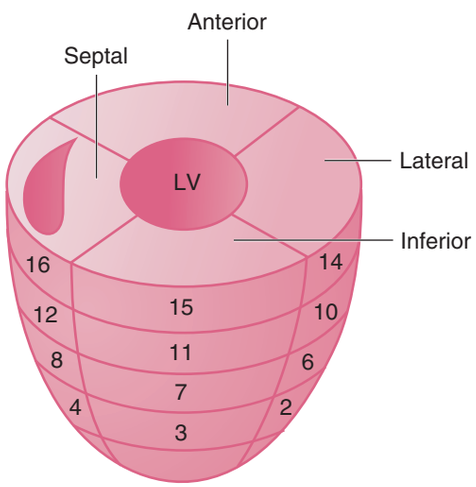

Figure 8.7 Diagram indicating the position of the myocardial tissue regions of interest.

ESTIMATION OF CARDIAC PERFUSION

The first objective of the canine studies was to determine whether the measurement of the kinetics of Tc-99m–teboroxime with dynamic cardiac SPECT is a more sensitive measure of ischemia than present static SPECT imaging with Tl-201. The second objective was to determine if the measurement of the kinetics of Tc-99m–teboroxime and Tl-201 could be used to simultaneously measure perfusion and viability.

Initial work was performed comparing Tc-99m–teboroxime dynamic SPECT with static Tl-201 imaging. Estimates of the washin of Tc-99m–teboroxime were compared to relative intensity measurements of Tl-201 for ROIs in the reconstructed short-axis slices shown in Figure 8.7. The myocardial tissue ROIs were drawn in six or seven short-axis slices. Each region was 7 mm thick and varied in size from 4 to 7 cm^3. It can be seen in Table 8.1 that the washin kinetic parameter correlates well with Tl-201 intensity. Additionally, washin provides a measure of perfusion times extraction. This is demonstrated in Figure 8.8, where estimates of washin are compared to microsphere flow measurements in the ROIs (corresponding to Fig. 8.7) for a canine study with occlusion. The results indicate a strong correlation between Tc-99m–teboroxime washin and Tl-201 intensity. Both were also shown to correlate with the microsphere data. The results suggest that estimates of the washin of Tc-99m–teboroxime can provide relative flow measurements with sensitivity comparable to that of Tl-201.

Later work was performed in canine cardiac perfusion studies comparing dynamic cardiac SPECT using Tc-99m–teboroxime and dynamic cardiac SPECT using Tl-201. Figure 8.9 shows the polar plots for the results. For both Tl-201 and Tc-99m–teboroxime, the washin parameters appear to give greater contrast than the summed data, which more closely represent a static

TABLE 8.1

Correlation of Technetium-99m–Teboroxime Washin to Thallium-201 Static Intensities in Canine Studies

Canine Study	Correlation (Washin to ^{201}Tl)
No occlusion	
1	0.713
2	0.735
3	0.837
Occlusion	
4	0.754
5	0.842
6	0.943

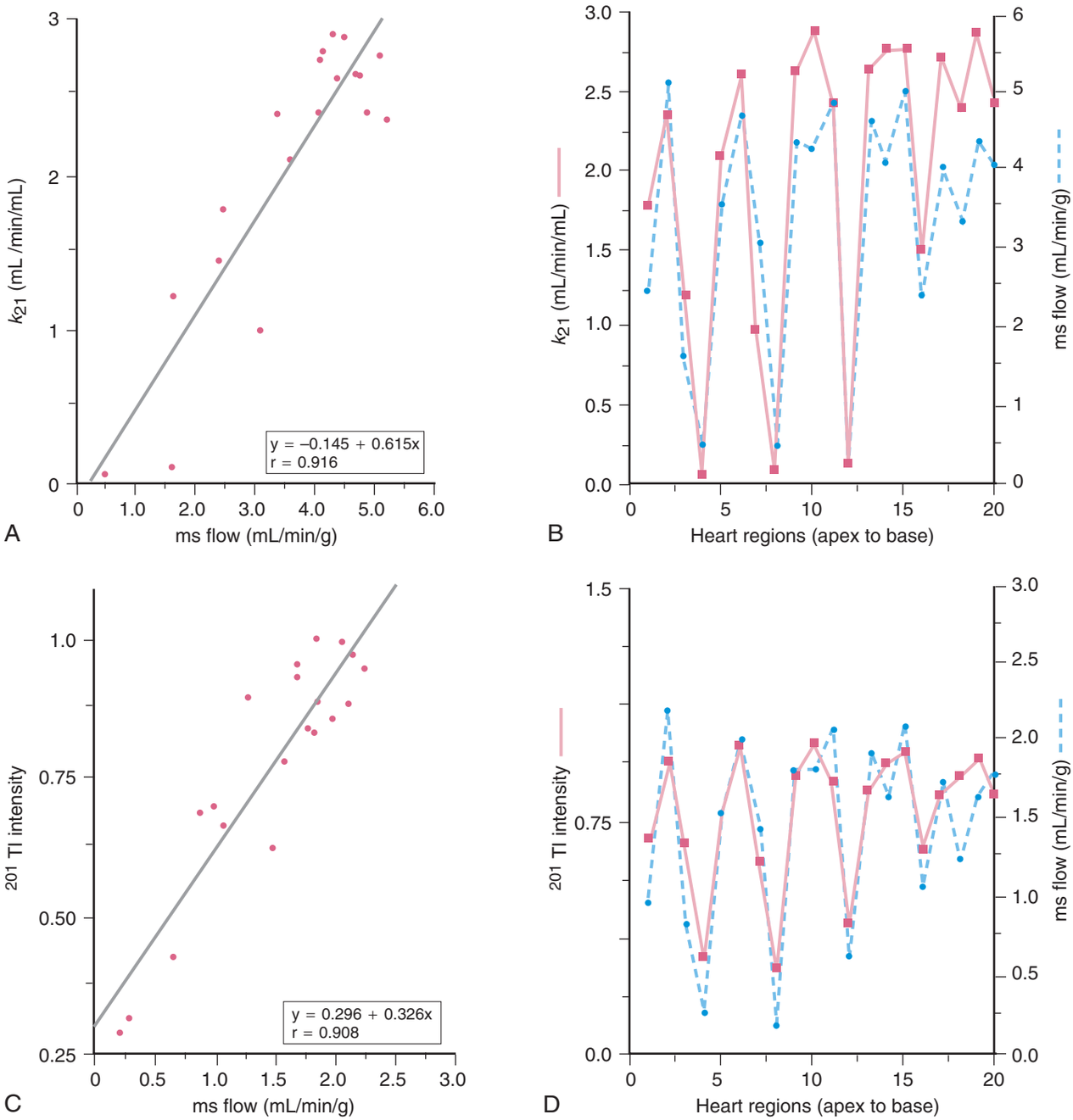

Figure 8.8 Results from an occluded canine study. *A*, Microsphere (ms) flow vs. estimates of washin (k_{21}) of Tc-99m–teboroxime from a stress scan; *B*, heart region vs. microsphere flow and estimates of washin; *C*, microsphere flow vs. Tl-201 intensity from the baseline scan; *D*, heart region vs. microsphere flow and Tl-201 intensity from the same baseline scan. A three-detector SPECT scanner (PRISM 3000, Picker International, Cleveland, Oh) was used to perform the scans. High-resolution fan beam collimators with a focal length of 65 cm were used. First, the transmission scan was performed. Immediately following the transmission scan, the stress Tl-201 scan was initiated. A second Tl-201 scan was performed at rest. Next, two Tc-99m–teboroxime dynamic SPECT scans were performed. First, a rest Tc-99m–teboroxime study was performed followed by a stress Tc-99m–teboroxime study. At the start of each scan, microspheres were injected to serve as a gold standard for blood flow.

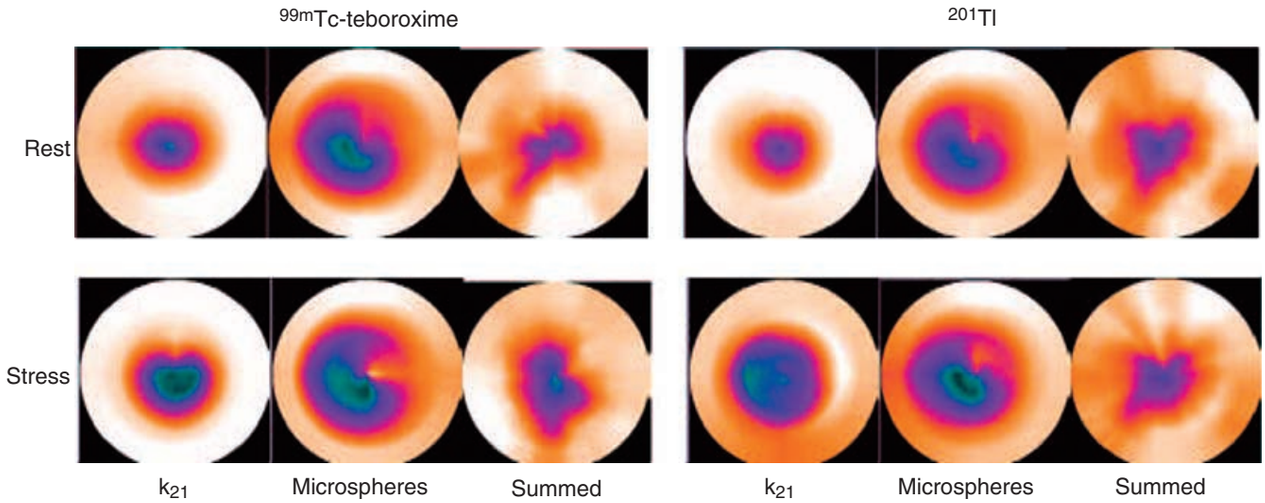

Figure 8.9 Polar plots comparing dynamic cardiac SPECT using Tc-99m–teboroxime and Tl-201 in a canine study. A canine weighing 30 kg was studied with the left anterior descending (LAD) artery occluded. The PRISM 3000XP with fan beam collimators (65 cm focal length) was used for data acquisition. Both transmission and emission acquisitions were performed. The dynamic Tl-201 and Tc-99m–teboroxime studies were obtained in the sequence: (1) stress Tl-201 (dose = 2.87 mCi), (2) rest Tl-201 study (dose = 1.48 mCi), (3) rest Tc-99m–teboroxime (dose = 22 mCi), and (4) stress Tc-99m–teboroxime (dose = 19.4 mCi). For the dynamic Tl-201 acquisitions 90 full sets of projection images [64 bins (0.712 cm pixels) ×64 slices ×120 angles] were obtained in two stages: the first, 60 frames of 10 seconds each; and the second, 30 frames of 60 seconds each. Adenosine was used to induce stress throughout the scan. For the dynamic Tc-99m–teboroxime acquisition 180 full sets of projection images [64 bins (0.712 cm pixels) ×64 slices ×120 angles] were obtained, each set of projections acquired every 5 seconds. Simultaneous with each radionuclide injection, microspheres were injected in the left atrium. The dynamic emission data were processed: First, static images for Tl-201 were obtained by summing up 20 minutes of the dynamic data beginning 10 min after injection. For ^{99m} Tc-teboroxime 10 minutes of dynamic data were summed beginning 2 minutes after injection. Second, both the Tc-99m–teboroxime and the Tl-201 static and dynamic data were reconstructed with the OSEM algorithm with attenuation and depth-dependent detector response correction. The blood and tissue time-activity curves were fit to a one-compartment model using RFIT.[97]

acquisition. Comparison of the results for Tl-201 and Tc-99m–teboroxime was somewhat surprising in that the Tl-201 washin parameter gave a better contrast than the Tc-99m–teboroxime washin parameter (some very excellent work on dynamic cardiac SPECT using Tl-201 was also performed by Eberl[74] and Iida[26]). Figure 8.10 shows the results in a patient study. Both the Tl-201 (Fig. 8.10*A*) and Tc-99m–teboroxime results (Fig. 8.10*D*) show a defect in the lateral wall. This is also seen in the polar plots. Increased liver activity is seen in the reconstructed Tc-99m–teboroxime images. The polar plots for the washin parameters show more contrast than the polar plots for the summed data for both Tl-201 and Tc-99m–teboroxime. In this particular study it appears that Tl-201 shows the greatest contrast, which may be due to presence of infarcted tissue, thus resulting in a decrease in adenosine triphosphate transport of Tl-201.

The study of myocardial perfusion is important in the study of several cardiac pathophysiologic abnormalities and provides the basis for therapeutic decisions on how best to treat such conditions. In addition to being the primary method for diagnosing myocardial ischemia, it is also important in the study of alterations in regional myocardial wall stress, strain, and material properties[115]; in the study of the relevance of endothelial dysfunction to physiologic flow control[116]; risk stratification that leads to sound, cost-effective treatment decisions by enabling clinicians to distinguish between high-risk patients who would likely benefit from invasive intervention from low-risk patients who would likely benefit from revascularization[117]; risk stratification of patients who arrive at the emergency department with symptoms suggestive of coronary artery disease (CAD) but have not had normal or nondiagnostic electrocardiograms[118]; and follow-up to revascularization, either through early-phase testing to demonstrate results of revascularization or late-phase testing to monitor patients for worsening CAD in unrevascularized areas (or in distal territories) and to identify bypass graft attrition.[119]

The use of stress nuclear myocardial perfusion imaging for risk stratification has evolved to become an established tool in the development of management strategies for patients with known or suspected coronary artery disease.[120]

ESTIMATION OF CARDIAC VIABILITY (see Chapters 31–34)

The *flow-function relation* is important clinically for distinguishing between conditions such as stunning, in

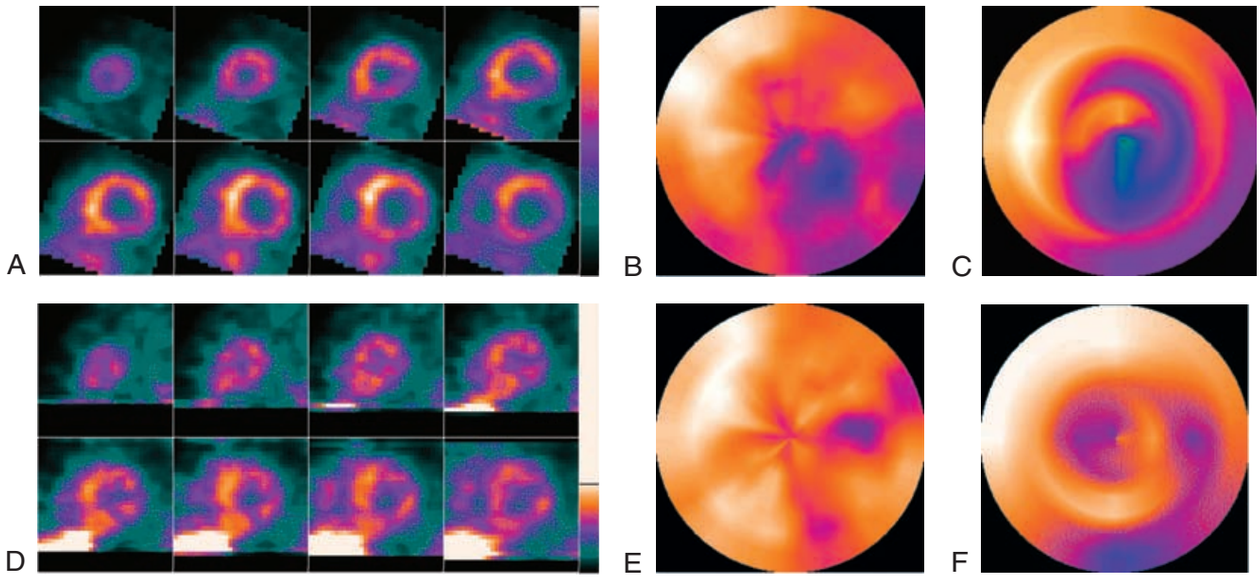

Figure 8.10 A patient study comparing Tl-201 and Tc-99m–teboroxime under stress conditions: *A*, reconstructed short-axis slices of the summed Tl-201 data; *B*, polar plot for the summed Tl-201 data; *C*, polar plot for the washin rate parameter for Tl-201; *D*, reconstructed short-axis slices of the summed Tc-99m–teboroxime data; *E*, polar plot for the summed Tc-99m–teboroxime data; and *F*, polar plot for the washin rate parameter for Tc-99m–teboroxime. The patient study was performed on the three-detector IRIX SPECT system equipped with parallel-hole collimators. Both the dynamic Tl-201 and dynamic Tc-99m–teboroxime studies were performed under pharmacologic stress using adenosine. The dynamic Tl-201 study was performed by infusing 3.02 mCi as a bolus. The acquisition consisted of two stages, 60 frames (120 projections/frame) of 11 seconds each and 60 frames (each 120 projections) of 30 seconds each. In the case of the dynamic Tc-99m–teboroxime study, 19.07 mCi was injected as a bolus. The acquisition consisted of 90 frames (120 projections/frame) each of 11 seconds' duration. The data were reconstructed with compensation for attenuation, detector response, and scatter. The summed static SPECT data for Tl-201 were obtained by skipping the initial 10-minute data and summing the subsequent 15 minutes. The teboroxime static SPECT data were obtained by skipping the initial 100 seconds of data and summing the subsequent 10 min. Cluster analysis was performed on eight short-axis slices of 0.5 cm to segment regions of interest for analysis.[73] Kinetic parameters were estimated from time-activity curves generated for the ROIs.

which function is depressed without abnormal perfusion, and hibernation, in which flow and function are both impaired.[115] Biopsy specimens taken from hibernating regions show structural degeneration characterized by reduced quantities of structural proteins, loss of myofilaments, and disorganization of the cytoskeleton, with varying degrees of replacement fibrosis.[121] In addition, apoptotic cells appear to be present and exhibit severe cellular degeneration.[121] Myocardial hibernation represents an incomplete adaptation to ischemia suggesting that myocardial necrosis will ultimately occur if blood flow is not restored.[122]

Not only is perfusion imaging used in evaluating cardiac viability and in risk stratification of patients for bypass surgery, but viable myocardium is also evaluated by studying ejection fraction, wall motion, and wall thickening of the left ventricular myocardium[123–125] or by studying its metabolic activity.[126–128] Gated SPECT is more often the method of choice for the evaluation of viable myocardium; which is usually done within a stress-rest protocol used to evaluate both perfusion and function simultaneously. However, metabolic imaging studies have shown that increased uptake of F-18-FDG is accompanied by a decrease in uptake of the fatty acid I-123–BMIPP.[126] The decreased uptake of the preferred substrate of fatty acid is evidence of myocardial ischemia. SPECT imaging of F-18-FDG simultaneous with Tc-99m–sestamibi has been shown to be useful for determining viable myocardium even in ischemic regions.[128]

Recently, we have been studying the effectiveness of dynamic cardiac SPECT for measuring viability, specifically by utilizing quantification of distribution volumes, which is the ratio of the rate of washin (k_{21}) over the rate of washout (k_{12}) of Tc-99m–teboroxime and Tl-201. A dynamic cardiac SPECT study was performed in a canine to evaluate myocardial viability and perfusion following occlusion and reperfusion. Triphenyl tetrazolium chloride (TTC) was used for determining viability, and radiolabeled microspheres were used as markers of myocardial blood flow during occlusion and after reperfusion.

Figure 8.11 shows the polar plots for the results of the dynamic Tc-99m–teboroxime studies. For one study, the microsphere data, the washin parameter estimates, the volume of distribution, and the TTC stained data are

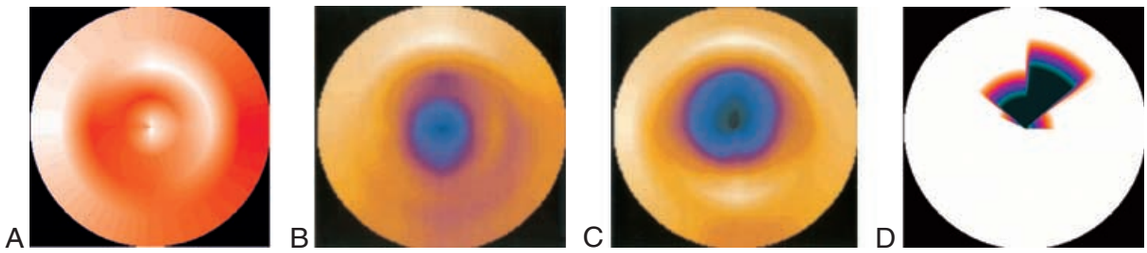

Figure 8.11 Canine reperfusion study performed with Tc-99m–teboroxime. Polar maps of: *A*, microsphere derived flows; *B*, washin parameter; *C*, volume of distribution (k_{21}/k_{12}); and *D*, threshold TTC data. In this study the LAD artery was occluded for approximately 150 minutes, then the occlusion was released and flow was allowed to perfuse the previously occluded region for 90 minutes before imaging was performed. The PRISM 3000XP SPECT system with fan beam collimators (65 cm focal length) was used for both transmission and emission imaging. After reperfusion, a dynamic Tc-99m–teboroxime SPECT study was performed at rest. Approximately 28 mCi (1036 MBq) of Tc-99m–teboroxime was injected simultaneously with the start of the dynamic acquisition. A dynamic sequence of 180 × 5.6 sec (120 projections/5.6 sec) was obtained during a total imaging time of 18 minutes. Simultaneous to the radionuclide injection, microspheres were injected into the left atrium. At the conclusion of the study, the canine was euthanized and the heart was sectioned into approximately six 7- to 10-mm short-axis slices and the slices were incubated in 1% triphenyltetrazolium (TTC) at 37°C for approximately 15–20 minutes. Photographs of the TTC-stained slices were taken: regions that were stained red were considered normal, and those that failed to stain were considered infarcted. The dynamic emission projection data were reconstructed using the OSEM algorithm with compensation for attenuation and detector response. A clustering technique[73] was used to select ROIs of short-axis slices for which time-activity curves were generated. The blood and tissue time-activity curves were fit to a one-compartment model using RFIT.[97] Parametric images were obtained for the washin (k_{21}) and the washout (k_{12}). The photographed slices were used to mark the TTC positive or negative regions on the image data and to register the microsphere data to the image data. Infarcted regions (0) considered were those that were not stained for more than 75% of the region, while the remaining region was considered to be normal region (1). A polar plot was obtained with 80 angles drawn for each slice and obtaining the intensity (0 or 1) for each region.

displayed. The washin parameter was used to reflect blood flow and was compared to the microsphere-derived blood flows. The volume of distribution was used to reflect viability. It was found that the microsphere flows were slightly higher in the apical regions than in the basal regions. It can be seen from the plots that the volume of distribution correlates with the TTC data. The results show that a decrease in washout correlates with an increase in TTC staining in the infarcted region. However, the microsphere-derived flow shows normal flow in the infarcted region, which correlates with normal washin rate parameters. This could be due to a hyperperfusion effect that has been reported in the literature in those cases where an occluded region has been reperfused, thus counteracting any reduced washin where there is presence of infarct, or it could be due to the fact that the washin of teboroxime is not significantly affected by infarcted tissue due to its high lipophilicity.

Figure 8.12 compares the volume of distribution for Tc-99m–teboroxime and Tl-201 for one of the canine studies. It appears that Tl-201 has a large area of

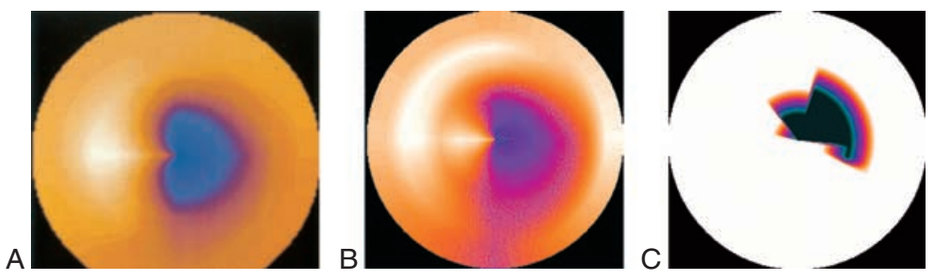

Figure 8.12 Canine reperfusion study comparing Tc-99m–teboroxime and Tl-201. Polar maps of: *A*, volume of distribution for Tc-99m–teboroxime; *B*, volume of distribution for Tl-201; and *C*, TTC data. The canine was prepared the same as that in Figure 8.11. After reperfusion, a dynamic Tc-99m–teboroxime SPECT study was performed at rest. Approximately 28 mCi of Tc-99m–teboroxime was injected simultaneously with the start of the dynamic acquisition. A dynamic sequence of 180 × 5.6 sec (120 projections/5.6 sec) was obtained during a total imaging time of 18 minutes. Then, a dynamic Tl-201 SPECT study was performed. Approximately 4 mCi of Tl-201 was injected simultaneously with the start of the dynamic acquisition. A dynamic sequence of 60 × 10 seconds, 30 × 60 seconds was obtained.

decreased volume of distribution indicating a larger region of nonviable tissue. We have seen this in other studies, which indicates that Tl-201 is more sensitive to mechanisms of metabolism, such as ATP-mediated membrane transport. Therefore, Tl-201 may provide a better contrast between viable and nonviable cardiac tissue. As can be seen in the previous canine study, the volume of distribution for both teboroxime and thallium may be a better measure of viability than the washin parameter.

There are no well-established processes for determining how and when to perform viability studies or how best to assess their benefits.[122] Only in a select few cases does surgical revascularization appear to afford a long-term survival benefit for patients with CAD and severe left ventricular (LV) dysfunction. Data suggest that viability assessment after myocardial infarction (MI) may be most beneficial among patients with LV dysfunction and minimal or no anginal symptoms. Whereas, viability assessment after myocardial infarction MI may be relatively less important in patients with low ejection fraction and severe angina with or without heart failure, as they appear to benefit from revascularization regardless of viability information, presumably through prevention of further loss of functioning myocytes and prevention of fatal ischemic events.[129] Thus, the goal of viability assessment is to identify patients for whom revascularization may potentially improve LV function. The determination should be made quickly because data suggest that prompt revascularization of hibernating myocardium will bestow faster and more complete restoration of LV function.

Noninvasive investigation of the amount of ischemia in viable myocardium is also an important component of the diagnostic evaluation of patients with severe LV dysfunction after MI. In acute myocardial infarction there are both local and diffuse microvascular consequences of the pathophysiology. Thus, an understanding of the status of the microvascular anatomy as well as microvascular function is important in evaluation of viable myocardium.[130] One way to accomplish this is to evaluate coronary flow reserve in viable myocardium.

ESTIMATION OF CORONARY FLOW RESERVE

(see Chapter 26)

The measure of coronary flow reserve (CFR) is becoming recognized as an important indicator of the physiologic significance of coronary stenoses as well as several other cardiac pathophysiologic conditions. CFR may provide early detection of arteriosclerosis both regionally and globally. CFR is defined as the ratio of coronary flow under maximal drug-induced hyperemia to baseline flow.[131] The measure of relative or absolute CFR has become an important physiologic parameter for detection and management of ischemic heart disease. Routine clinical SPECT imaging provides a simple noninvasive method for assessing relative regional CFR.[132] However, true quantitation of CFR has thus far been limited to other modalities[133–135] that include invasive methods such as intravascular Doppler ultrasound[136] or noninvasive methods such as transthoracic ultrasound,[137] magnetic resonance imaging (MRI),[138] and PET.[37,46,47] PET with [^{15}O]-labeled water is the noninvasive gold standard for obtaining quantitative regional blood flows[52]; however, the measurement of CFR has also been performed by using PET with N-13-ammonia[46,47] and with Rb-82.[37] The regional CFR is computed using the stress/rest ratio of flows calculated using quantitative compartmental analysis. Evidence is accumulating that high-resolution, accurate measurements of CFR can be obtained, and may be significantly more valuable than the relative CFR measurements that are obtained with current clinical SPECT methods. It is anticipated that modified SPECT acquisition and processing will be able to provide absolute CFR measurements.

A recent editorial gives more details, including use of dynamic SPECT for measuring absolute CFR.[32] Specifically, it was mentioned that Sugihara and colleagues[139] presented a noninvasive method of obtaining CFR using planar and SPECT imaging with Tc-99m–tetrofosmin. The approach is a "microsphere" method; it is assumed that the tracer sticks in the myocardial tissue so that myocardial flow (mL/min/g) can be calculated as the ratio of the counts in the tissue over the integral of the arterial concentration of the tracer up to the time of the SPECT measurement. Serial planar imaging is performed to obtain images of the first transit through the pulmonary artery, which is used to give a measure of the arterial concentration. SPECT is performed to provide counts in the region of interest. The method is performed both at rest and under induced stress. In healthy subjects, a CFR measurement of 1.47 was obtained. The CFR is significantly decreased in an infarcted region with a CFR of 1.08 and in an ischemic region with a CFR of 1.11.

Another approach is to use dynamic cardiac SPECT[9] with an agent such as Tc-99m–teboroxime to calculate CFR. The methods are similar to those used in dynamic PET. We have calculated both regional and global CFR measurements in canines and in patients using the ratio of the washin for adenosine-induced coronary vasodilatation (stress) to the washin at baseline flow (rest) as the CFR measurement. Our regional measurements for two subjects diagnosed as normal ranged from 1.6 to 2.3 with a global measurement of 1.9. Our results show that a patient with two-vessel disease had regional CFRs ranging between 1 and 1.2 with a global CFR of 1.09, and a patient with three-vessel disease had regional CFRs ranging between 0.64 and 1.2 with a global CFR of 0.94. These results are similar to those of Sugihara

and colleagues[139] but are somewhat lower than those previously reported by Chiao and colleagues.[30] They reported global CFR measurements (ratio of washin of Tc-99m–teboroxime at stress to that of rest) in healthy individuals that ranged from 1.19 to 3.87 with a mean of 3.44 ± 1.07. PET studies using $^{13}NH_3$ give even greater values, as high as 4.3 ± 1.6.[42]

Comments and references. Thallium-201 is often considered to be an analog of potassium; however, thallium differs from potassium in a number of characteristics. Thallium-201 has been widely used for cardiac SPECT imaging because of its somewhat desirable kinetics and capacity to "redistribute" well. However, Tc-99m–labeled agents, such as sestamibi,[13–16,18,19] have better photon energy for gamma imaging, shorter half-life, and reduced scatter. The Tc-99m–teboroxime radiopharmaceutical was developed to replace Tl-201 as a new tracer for imaging myocardial ischemia.[9,140–146] Technetium-99m–teboroxime (Cardio-Tec, Bracco, Princeton, NJ) is a boronic acid Tc-99m–labeled dioxime (BATO) complex that is stable, neutral, and lipid soluble, which is more diffusible and has a faster clearance time from the myocardium (half-life of 10–15 minutes)[140] than either Tl-201 or Tc-99m–sestamibi, and has the least degree of sensitivity to cellular dysfunction. It is 80%–90% extracted in the first pass.[140] Dynamic SPECT will make Tc-99m–teboroxime more useful as a flow agent and will better use both Tc-99m–teboroxime and Tl-201 as a marker of viability. Our results[29,31] and those of Iida and Eberl[26] demonstrate that Tl-201 correlates well with flow but has a flow times extraction less than that of Tc-99m–teboroxime, which may be an indication that the distribution of Tl-201 is facilitated by active transport and thus indicates that Tl-201 may be better for evaluating viability than Tc-99m–teboroxime. The literature is somewhat mixed on whether teboroxime is useful for imaging cellular dysfunction,[144] but differences between Tl-201 and Tc-99m–teboroxime in classifying infarct and infarct/ischemia are apparent.[9] Disadvantages for using tetrofosmin for CFR measurements may be due to the limited extraction of Tc-99m–tetrofosmin at high blood flow,[139] and tetrofosmin's interaction with red blood cells and plasma proteins may create difficulty in obtaining a true input function. Global CFR is a useful indicator; but in practice a single number is not useful when vessel-specific or region-specific CFR measurements are desired.[134] Unfortunately, regional myocardial dysfunction associated with infarction or regional ischemia may also impair CFR in remote regions with no presence of a coronary stenosis.[147] A number of disease processes may impair vascular reserve in small, isolated nontransmural regions of the myocardium. Current approaches to assessing CFR cannot effectively identify CFR changes in the endocardium and epicardium, although the ability to measure CFR selectively in the subendocardium may be possible given recent advancements in MRI.[138] Another important issue that arises when applying vasodilators is whether maximum vasodilatation has been achieved.[134] It has been pointed out that it may be difficult to obtain accurate CFR due to changes of heart rate at rest.[148] The method presented by Sugihara and colleagues[139] works only for radiopharmaceuticals that act like "microspheres," which do not wash out from the tissue from the time of injection to the time of measurement. Dynamic cardiac SPECT works best with radiopharmaceuticals that have high extraction. Other issues addressed in our studies include (1) the effect of photon statistics on variability of estimates of washin,[62] (2) the effect of cardiac motion on parameter estimates,[149] (3) the effect of partial volume on parameter estimates,[56] (4) the variability of flow in the myocardium,[150] and (5) input function shape and image acquisition interval.[62]

Future Directions

This chapter highlights some of the important compartment modeling and data processing aspects of dynamic cardiac SPECT (for fast data acquisition).

1. In dynamic cardiac SPECT the principle of tracer kinetics is used to extract kinetic parameters of compartment models that describe the pathways and dynamic behavior of tracers in cardiac tissue. Defect contrast is better evaluated with washin parameters obtained from dynamic Tc-99m–teboroxime and Tl-201 data and compartmental modeling methods.

2. Kinetic modeling of dynamic SPECT data involves a complex multivariable nonlinear estimation problem.[109] Iterative reconstruction algorithms are usually performed to reconstruct each dynamic three-dimensional distribution. The algorithms correct for attenuation, scatter, and the spatially varying geometric point response. The iterative approach can also provide estimates of the reconstructed errors. Kinetic parameters and errors are more accurate when the full covariance matrix of the sampled data (including both reconstructed sampled blood and tissue data) is used as a weighting matrix rather than ignoring the errors and using a weighting matrix of equal errors in the fitting procedure.[98] With today's computers, it is now possible to obtain reconstructions and error estimates from direct matrix inversion using singular value decomposition (SVD) of matrices.[96,103]

3. It was demonstrated that dynamic cardiac SPECT is able to obtain parametric images at the resolution of conventional cardiac SPECT images (see section Esti-

mation of Parametric Images). An important breakthrough in this work was being able to develop methods for extracting automatically blood time-activity curves from the data without having to draw ROIs. This is done by extracting unique factors and factor coefficients from dynamic reconstructed data using maximum entropy techniques, postprocessing methods that use physiologic constraints, and least-squares techniques with penalty terms that encourage factors to be positive and orthogonal.[110] These methods were successfully applied to the important clinical problem of eliminating liver activity that overlaps the inferior wall of the left ventricle in Tc-99m–teboroxime studies.[112]

4. Results of canine experiments were presented that demonstrate that dynamic cardiac SPECT is able to obtain estimates of flow kinetics using Tc-99m–teboroxime and Tl-201. An important key result emerging from this work is that the washin parameters of Tc-99m–teboroxime and Tl-201 provide greater defect contrast than can be obtained with static imaging of these radiopharmaceuticals.[27,31] It is anticipated that the estimation of kinetic parameters will yield greater dynamic range than the mapping of flow that is based on the intensity uptake of the radiopharmaceutical from a static study, which is the method typically used with Tl-201 to detect ischemia or infarct. Dynamic cardiac SPECT not only enhances the capability of Tl-201 to measure tissue viability but it also makes it possible for Tc-99m–teboroxime to measure tissue viability, which was thought impossible when investigated using static cardiac perfusion SPECT. It is known that Tc-99m–teboroxime follows flow linearly over a longer range of flows than does either Tl-201 or Tc-99m–sestamibi. This means that the use of dynamic SPECT with Tc-99m–teboroxime may be better to predict coronary flow reserve using a rest and a stress study.

What would be the best tracer for dynamic cardiac SPECT? In PET, $H_2{}^{15}O$ and $^{13}NH_3$ are most often used for measuring CFR, but there have been some reports of using Rb-82.[37] $H_2{}^{15}O$ is preferred because of its high extraction and linearity of uptake with flow, even at high flows associated with pharmacological stress. However, an additional inhalation of $C^{15}O$, which tags to hemoglobin, is needed to subtract the high concentration in the blood pool from the tissue. In SPECT, the results of Chiao and colleagues[30] show that washin and washout estimates of Tc-99m–teboroxime for the entire left ventricular myocardium changed significantly in response to coronary vasodilatation. Therefore, quantitative compartmental analysis of Tc-99m–teboroxime kinetics provides a sensitive indicator for changes in estimates of washin in response to adenosine-induced coronary vasodilatation. Our results corroborate these findings. In addition, we show that dynamic imaging of teboroxime with compartment modeling provides a better measure of flow (better contrast) than can be obtained from static imaging of Tl-201,[31] or for that matter, static imaging of Tc-99m–teboroxime.[31] In fact, dynamic SPECT may provide advantages, because it may enable better measurement of both perfusion and viability. Dynamic cardiac SPECT imaging with Tl-201 could potentially be useful for measuring CFR, but a flow agent is needed with a larger range of flow values for which the extraction fraction remains linear as a function of flow.

There are several possible tracers that can be used as *chemical "microspheres."* The agent Tc-99m–tetrofosmin showed promising initial results for calculating CFR using a single-detector SPECT system.[139] Technetium-99m–tetrofosmin has an extraction fraction less than another commonly used diffusible radiotracer, Tc-99m–sestamibi. It has been suggested that Tc-99m–sestamibi is also a possible tracer for calculating CFR using this "microsphere" technique.[139] Iodorotenone[151] is another potential agent that has an even a higher extraction fraction than these commonly used compounds, and may also be a useful tracer for calculating CFR. Further work is required to evaluate the "microsphere" method for calculating CFR in comparison with dynamic SPECT and dynamic PET imaging of agents with fast turnover.

In addition, the dynamic SPECT methods developed may be useful for evaluating myocardial function using other tracers, such as the glucose analog F-18-FDG,[96] the fatty acid I-123-IPPA,[96] and Tc-99m–N-NOET.[152] The agent Tc-99m–N-NOET has features of greater redistribution and linearity with flow, persistent with a higher level of hyperemia than any current agent but has not been introduced because of other physical disadvantages. Technetium-99m–N-NOET is a neutral compound like Tc-99m–teboroxime, with slower myocardial clearance, which makes this agent a potential better alternative for dynamic cardiac SPECT imaging than either Tl-201 or Tc-99m–teboroxime.

Further work is needed in the following areas:

1. Determine how dynamic SPECT approaches for measuring perfusion defects, viable tissue, and CFR can be better evaluated and tested in humans. Specifically, systematic studies should be done to define the distribution of absolute CFR in both normal and abnormal hearts, and to determine how the common factors that can diminish CFR affect regional reserve, especially in small subendocardial regions.

2. Develop better perfusion and metabolic tracers and provide easier access to present perfusion and metabolic tracers.

3. Create technological advances that improve SPECT imaging systems so that they better facilitate dynamic imaging. In the past, SPECT systems have been limited by low sensitivity, and poor spatial and temporal resolution, as a result of the necessary mechanical rotation of the detector. Ideally, dynamic imaging is best accomplished by a multidetector or ring system.
4. Make improvements in data acquisition. Manufacturers need to provide list mode acquisition on all SPECT camera systems with timing marks, and electrocardiographic and respiratory gating signatures.
5. Provide improved computing hardware. The manufacturers need to supply computer hardware and disk storage that will allow for the processing and storage of large dynamic data sets.
6. Develop automated data analysis techniques. A critical component in the analysis of dynamic cardiac SPECT data is the successful extraction of time-activity curves for ROIs in the blood and heart tissue. Automatic data segmentation techniques are vital for the processing of dynamic SPECT data because of the large amount of data, which makes it essential to minimize operator involvement, and for efficient production of accurate and reproducible results within a study as well as between studies performed at other times.
7. Develop data processing techniques to estimate kinetic parameters directly from projection data acquired from SPECT systems with rotating detectors.
8. Develop accurate models of the physics (attenuation, scatter, and depth-dependent resolution) of the image detection process. The development of better models will improve the bias of the estimated kinetic parameters. Also, it is important to accelerate the computation of these algorithms so that they are clinically feasible.
9. Develop data processing techniques to simultaneous model cardiac deformation and tracer kinetics. Cardiac motion, lung motion, and patient motion tend to mix the blood and tissue in the input blood ROI biasing the estimates of the model parameters.[96] Also, accurate measure of wall motion is important for determining viable myocardial tissue.
10. Perform dynamic imaging for every cardiac study. Allow for dynamic acquisition where the acquired data can be reformatted to provide a conventional imaging data set. The input function can then be used to normalize results, which is important for comparisons with follow-up studies.

In summary, SPECT has become an important diagnostic tool in cardiovascular nuclear medicine, and the role of radionuclide procedures using SPECT for diagnosis and therapeutic planning continues to grow. Because cardiovascular disease continues to be prevalent in the population, those tests that allow noninvasive assessment of cardiac function, such as those involving dynamic cardiac SPECT, will continue to play an important role in clinical nuclear medicine. Our results[27–29,31] and those of others[26,30] have demonstrated that dynamic cardiac SPECT allows for more versatility in probing the physiologic properties of the myocardium and better utilization of the diagnostic potential of Tc-99m–teboroxime and Tl-201, and may be a more sensitive measure of ischemia and viability than static imaging of these perfusion agents. The further development of dynamic cardiac SPECT is essential to fully use the potential that agents, such as Tc-99m–teboroxime, offer for human use. With proper attention to data acquisition and the processing of dynamic data, information about kinetic parameters can be obtained from noisy data sets, which will make dynamic SPECT a useful tool in clinical nuclear cardiology.

Dynamic SPECT imaging is exploring a new frontier in medical imaging, which involves the development of new imaging hardware, radiopharmaceuticals, and data processing algorithms. Its development has significant implications not only for advancing nuclear cardiology but also for improving the imaging of cardiac and other organ systems with all imaging modalities. The progress made in dynamic SPECT imaging has potential for new applications, such as in imaging other organ systems such as the brain[153] and kidneys,[111,154,155] and in imaging tumors to differentiate malignant and benign tissue. The opportunities also include repeated brain activation studies, pulmonary transaxial function studies,[156,157] and other organ studies that include applications of metabolism and receptor binding. The mathematical tools developed may also have significant implications for application to other imaging modalities such as the analysis of MRI kinetic data of the perfusion of endogenous excited protons,[158,159] and the analysis of dynamic x-ray CT dynamic data of the perfusion of contrast media.

Acknowledgments

The research presented in this chapter was partially supported by NIH Grant No. RO1 HL 39792 and by the Director, Office of Science, Office of Biological and Environmental Research, Medical Sciences Division of the U.S. Department of Energy, under contract DE-ACO3-76SF00098. The authors thank Harshali Bal for processing the canine and patient studies and Arkadiusz Sitek, PhD, for providing the parametric images in Figure 8.6. The authors also thank Dr. Elias Botvinick for his helpful

discussions. Also, the authors appreciate the careful proofreading of the manuscript by Sean Webb.

References

1. Botvinick E (ed): *Self Study Program III—Nuclear Medicine: Cardiology Topic 6—Myocardial Perfusion Scintigraphy By Single Photon Radionuclides—Planar And Tomographic (SPECT)—Clinical Aspects*. Reston, Md: Society of Nuclear Medicine.
2. Budinger TF, Cahoon JL, Derenzo SE, et al: Three dimensional imaging of the myocardium with radionuclides. *Radiology* 125:433–439, 1977.
3. Ritchie JL, Williams DL, Harp G, et al: Transaxial tomography with thallium-201 for detecting remote myocardial infarction. *Am J Cardiol* 50:1236–1241, 1982.
4. Maulblant J, Cassagnes J, LeJeune J, et al: A comparison between conventional scintigraphy and emission tomography with thallium-201 in the detection of myocardial infarction: Concise communication. *J Nucl Med* 23:204–208, 1982.
5. Garcia EV, Van Train K, Maddahi J, et al: Quantification of rotational thallium-201 myocardial tomography. *J Nucl Med* 26:17–26, 1985.
6. McPhee SJ, Garnick DW: Imaging the heart: Cardiac scintigraphy and echocardiography in U.S. hospitals (1983). *J Nucl Med* 27:1635–1641, 1986.
7. Datz FL, Gullberg GT, Gabor FV, et al: SPECT myocardial perfusion imaging update. *Semin Ultrasound CT MR* 12:28–44, 1991.
8. Datz FL, Gabor FV, Christian PE, et al: The use of computer-assisted diagnosis in cardiac perfusion nuclear medicine studies: A review (Part I). *J Digital Imag* 5:209–222, 1992.
9. Serafini AN, Topchik S, Jimenez H, et al: Clinical comparison of technetium-99m-teboroxime and thallium-201 utilizing a continuous SPECT imaging protocol. *J Nucl Med* 33:1304–1311, 1992.
10. Allman KC, Berry J, Sucharski LA, et al: Determination of extent and location of coronary artery disease in patients without prior myocardial infarction by thallium-201 tomography with pharmacologic stress. *J Nucl Med* 33:2067–2073, 1992.
11. Datz FL, Gabor FV, Christian PE, et al: The use of computer-assisted diagnosis in cardiac perfusion nuclear medicine studies: A review (Part II). *J Digital Imag* 6:1–15, 1993.
12. Datz FL, Rosenberg C, Gabor FV, et al: The use of computer-assisted diagnosis in cardiac perfusion nuclear medicine studies: A review (Part III). *J Digital Imag* 6:67–80, 1993.
13. Mannting F, Morgan-Mannting MG: Gated SPECT with technetium-99m-sestamibi for assessment of myocardial perfusion abnormalities. *J Nucl Med* 34:601–608, 1993.
14. Gunalp B, Dokumaci B, Uyan C, et al: Value of dobutamine technetium-99m-sestamibi SPECT and echocardiography in the detection of coronary artery disease compared with coronary angiography. *J Nucl Med* 34:889–894, 1993.
15. Datz FL, Gullberg GT, Zeng GL, et al: Application of convergent-beam collimation and simultaneous transmission emission tomography to cardiac SPECT imaging. *Semin Nucl Med* 24:17–37, 1994.
16. Williams KA, Taillon LA: Reversible ischemia in severe stress technetium 99m-labeled sestamibi perfusion defects assessed from gated single-photon emission computed tomographic polar map Fourier analysis. *J Nucl Cardiol* 2:199–206, 1995.
17. Gioia G, Milan E, Giubbini R, et al: Prognostic value of tomographic rest-redistribution thallium 201 imaging in medically treated patients ventricular dysfunction. *J Nucl Cardiol* 3:150–156, 1996.
18. Maunoury C, Chen CC, Chua KB, et al: Quantification of left ventricular function with thallium-201 and technetium-99m-sestamibi myocardial gated SPECT. *J Nucl Med* 38:958–961, 1996.
19. Flamen P, Bossuyt A, Franken PR: Technetium-99m-tetrofosmin in dipyridamole-stress myocardial SPECT imaging: Intraindividual comparison with technetium-99m-sestamibi. *J Nucl Med* 36:2009–2015, 1995.
20. Krishnan R, Lu J, Dae MW, et al: Does myocardial perfusion scintigraphy demonstrate clinical utility in patients with markedly positive exercise test?—An assessment of the method in a high risk subset. *Am Heart J* 127:804–815, 1993.
21. Heller GV, Herman SD, Travin MI, et al: Independent prognostic value of intravenous dipyridamole with technetium-99m sestamibi tomographic imaging in predicting cardiac events and cardiac-related hospital admissions. *J Am Coll Cardiol* 26:1202–1208, 1995.
22. Berman DS, Hachamovitch R, Kiat H, et al: Incremental value of prognostic testing in patients with known or suspected ischemic heart disease: A basis for optimal utilization of exercise technetium-99m sestamibi myocardial perfusion single-photon emission computed tomography. *J Am Coll Cardiol* 26:639–647, 1995.
23. Hachamovitch R, Berman DS, Kiat H, et al: Comparison of incremental prognostic value, risk stratification and cost effectiveness of rest/exercise Tl-201/Tc-99m sestamibi SPECT in women and men. *J Am Coll Cardiol* 28:34–44, 1996.
24. Sharir T, Germano G, Kavanagh PB, et al: Incremental prognostic value of post-stress left ventricular ejection fraction and volume by gated myocardial perfusion single photon emission computed tomography. *Circulation* 100:1035–1042, 1999.
25. Shaw LJ, Hachamovitch R, Berman DS, et al: The economic consequences of available diagnostic and prognostic strategies for the evaluation of stable angina patients: An observation assessment of the value of precatherization ischemia. For the Economics of Noninvasive Diagnosis (END) Multicenter Study Group. *J Am Coll Cardiol* 33:661–669, 1999.
26. Iida H, Eberl S: Quantitative assessment of regional myocardial blood flow with thallium-201 and SPECT. *J Nucl Cardiol* 5:313–331, 1998.
27. Khare HS, Di Bella EVR, Kadrmas DJ, et al: Comparison of static and dynamic cardiac perfusion thallium-201 SPECT. *IEEE Trans Nucl Sci* 48:774–779, 2001.
28. Smith AM, Gullberg GT, Christian PE, et al: Kinetic modeling of teboroxime using dynamic SPECT imaging of a canine model. *J Nucl Med* 35:484–495, 1994.
29. Smith AM, Gullberg GT, Christian PE: Experimental verification of technetium 99m-labeled teboroxime kinetic parameters in the myocardium with dynamic single-photon emission computed tomography: Reproducibility, correlation to flow, and susceptibility to extravascular contamination. *J Nucl Cardiol* 3:130–142, 1996.
30. Chiao P-C, Ficaro EP, Dayanikli F, et al: Compartmental analysis of technetium-99m-teboroxime kinetics employing fast dynamic SPECT at rest and stress. *J Nucl Med* 35:1265–1273, 1994.
31. Di Bella EVR, Ross SG, Kadrmas DJ, et al: Compartmental modeling of technetium-99m-labeled teboroxime with dynamic single-photon emission computed tomography: Comparison to static thallium-201 in a canine model. *Inv Radiol* 36:178–185, 2001.
32. Gullberg GT, Di Bella EVR, Sinusas A: Editorial—Estimation of coronary flow reserve: Can SPECT compete with other modalities? *J Nucl Cardiol* 8:620–625, 2001.
33. Budinger TF, Yano Y, Hoop Jr B: A comparison of ^{82}Rb and ^{13}NH for myocardial positron scintigraphy. *J Nucl Med* 16:429–431, 1975.
34. Yano Y, Chu P, Budinger TF: Rubidium-82 generators for imaging studies. *J Nucl Med* 18:46–50, 1977.

35. Mullani NA, Goldstein RA, Gould KL, et al: Myocardial perfusion with rubidium-82. I. Measurement of extraction fraction and flow with external detectors. *J Nucl Med* 24:898–906, 1983.
36. Goldstein RA, Mullani NA, Marani SK, et al: Myocardial perfusion with rubidium-82. II. Effects of metabolic and pharmacologic interventions *J Nucl Med* 24:907–915, 1983.
37. Gould KL, Goldstein RA, Mullani NA, et al: Noninvasive assessment of coronary stenoses by myocardial perfusion imaging during pharmacologic coronary vasodilation. VIII. Clinical feasibility of positron cardiac imaging without a cyclotron using generator-produced rubidium-82. *J Am Coll Cardiol* 7:775–789, 1986.
38. Herrero P, Markham J, Shelton ME, et al: Implementation and evaluation of a two-compartment model for quantification of myocardial perfusion with rubidium-82 and positron emission tomography. *Circ Res* 70:496–507, 1992.
39. MacIntyre WJ, Go RT, King JL, et al: Clinical outcome of cardiac patients with negative thallium-201 SPECT and positive rubidium-82 PET myocardial perfusion imaging. *J Nucl Med* 34:400–404, 1993.
40. Krivokapich J, Huang S-C, Phelps ME, et al: Dependence of ^{13}NH3 myocardial extraction and clearance on flow and metabolism. *Am J Physiol* 242:H536–H542, 1982.
41. Krivokapich J, Smith GT, Huang S-C, et al: ^{13}N ammonia myocardial imaging at rest and with exercise in normal volunteers—Quantification of absolute myocardial perfusion with dynamic positron emission tomography. *Circulation* 80:1328–1337, 1989.
42. Hutchins GD, Schwaiger M, Rosenspire KC, et al: Noninvasive quantification of regional blood flow in the human heart using N-13 ammonia and dynamic positron emission tomographic imaging. *J Am Coll Cardiol* 15:1032–1042, 1990.
43. Hara T, Michihata T, Yokoi F, et al: Quantitative measurement of regional myocardial blood flow in patients with coronary artery disease by intravenous injection of ^{13}N-ammonia in positron emission tomography. *Eur J Nucl Med* 16:231–235, 1990.
44. Kuhle WG, Porenta G, Huang S-C, et al: Quantification of regional myocardial blood flow using ^{13}N-ammonia and reoriented dynamic positron emission tomographic imaging. *Circulation* 86:1004–1017, 1992.
45. Muzik O, Beanlands RSB, Hutchins GD, et al: Validation of nitrogen-13-ammonia tracer kinetic model for quantification of myocardial blood flow using PET. *J Nucl Med* 34:83–91, 1993.
46. Masuda D, Nohara R, Tamaki N, et al: Evaluation of coronary blood flow reserve by ^{13}N-NH_3 positron emission computed tomography (PET) with dipyridamole in the treatment of hypertension with the ACE inhibitor (Cilazapril). *Ann Nucl Med* 14:353–360, 2000.
47. Yokoyama I, Ohtake T, Momomura S, et al: Reduced coronary flow reserve in hypercholesterolemic patients without overt coronary stenosis. *Circulation* 94:3232–3238, 1996.
48. Huang SC, Schwaiger M, Carson RE, et al: Quantitative measurement of myocardial blood flow with oxygen-15 water and positron computed tomography: An assessment of potential and problems. *J Nucl Med* 26:616–625, 1985.
49. Bergmann SR, Herrero P, Markham J, et al: Noninvasive quantitation of myocardial blood flow in human subjects with oxygen-15-labeled water and positron emission tomography. *J Am Coll Cardiol* 14:639–652, 1989.
50. Araujo LI, Lammertsma AA, Rhodes CG, et al: Noninvasive quantification of regional myocardial blood flow in coronary artery disease with oxygen-15-labeled carbon dioxide inhalation and positron emission tomography. *Circulation* 83:875–885, 1991.
51. Iida H, Rhodes CG, de Silva R, et al: Use of the left ventricular time-activity curve as a noninvasive input function in dynamic oxygen-15-water positron emission tomography. *J Nucl Med* 33:1669–1677, 1992.
52. Pitkanen OP, Raitakari OT, Ronnemaa T, et al: Influence of cardiovascular risk status on coronary flow reserve in healthy young men. *Am J Cardiol* 79:1690–1692, 1997.
53. Smith AM, Gullberg GT: Dynamic cardiac SPECT computer simulations for teboroxime kinetics. *IEEE Trans Nucl Sci* 41:1626–1633, 1994.
54. Feng D, Li X, Huang SC: A new double modeling approach for dynamic cardiac PET studies using noise and spillover contaminated LV measurements. *IEEE TransBiomed Engin* 43:319–327, 1996.
55. Hutchins GD, Caraher JM, Raylman RR: A region of interest strategy for minimizing resolution distortions in quantitative myocardial PET studies. *J Nucl Med* 33:1243–1250, 1992.
56. Welch A, Smith AM, Gullberg GT: An investigation of the effect of finite system resolution and photon noise on the bias and precision of dynamic cardiac SPECT parameters. *Med Phys* 22:1829–1836, 1995.
57. Hutton BF, Osiecki A: Correction of errors due to partial volume effects including contractile movement in resting myocardial SPECT (abstract). *J Nucl Med* 37:215P, 1996.
58. Rhodes CG, Wollmer P, Fazio F, et al: Quantitative measurement of regional extravascular lung density using positron emission and transmission tomography. *J Comput Assist Tomog* 5:783–791, 1981.
59. Rumsey WL, Rosenspine KC, Nunn AD: Myocardial extraction of teboroxime: Effects of teboroxime interaction with blood. *J Nucl Med* 33:94–101, 1992.
60. Mazoyer BM, Huesman RH, Budinger TF, et al: Dynamic PET data analysis. *J Comput Assist Tomogr* 10:645–653, 1986.
61. Raylman RR, Caraher JM, Hutchins GD: Sampling requirements for dynamic cardiac PET studies using image-derived input functions. *J Nucl Med* 34:440–447, 1993.
62. Ross SG, Welch A, Gullberg GT, et al: An investigation into the effect of input function shape and image acquisition interval on estimates of washin for dynamic cardiac SPECT. *Phys Med Biol* 42:2193–2213, 1997.
63. Lau CH, Eberl S, Feng D, et al: Optimized acquisition time and image sampling for dynamic SPECT of Tl-201. *IEEE Trans Med Imag* 17:334–343, 1998.
64. Links JM, Frank TL, Becker LC: Effect of differential tracer washout during SPECT acquisition. *J Nucl Med* 32:2253–2257, 1991.
65. O'Connor MK, Cho DS: Rapid radiotracer washout from the heart: Effect on image quality in SPECT performed with a single-headed gamma camera system. *J Nucl Med* 33:1146–1151, 1992.
66. Reutter BW, Gullberg GT, Huesman RH: Kinetic parameter estimation from attenuated SPECT projection measurements. *IEEE Trans Nucl Sci* 45:3007–3013, 1998.
67. Reutter BW, Gullberg GT, Huesman RH: Direct least squares estimation of spatiotemporal distributions from dynamic SPECT projections using a spatial segmentation and temporal B-splines. *IEEE Trans Med Imag* 19:434–450, 2000.

67A. Reutter BW, Gullberg GT, Huesman RH: Accuracy and precision of compartmental model parameters obtained from directly estimated dynamic SPECT time-activity curves. *IEEE Trans Nucl Sci* 51:170–176, 2004.

68. Stewart RE, Schwaiger M, Hutchins GD, et al: Myocardial clearance kinetics of technetium-99m-SQ30217: A marker of regional myocardial blood flow. *J Nucl Med* 31:1183–1190, 1990.
69. Nakajima K, Taki J, Bunko H, et al: Dynamic acquisition with a three-headed SPECT system: Application to technetium

99m-SQ30217 myocardial imaging. *J Nucl Med* 32:1273–1277, 1991.
70. Chua T, Kiat H, Germano G, et al: Rapid back to back adenosine stress/rest technetium-99m teboroxime myocardial perfusion SPECT using a triple-detector camera. *J Nucl Med* 34:1485–1493, 1993.
71. Budinger TF, Araujo L, Ranger N, et al: Dynamic SPECT feasibility studies (abstract). *J Nucl Med* 32:955, 1991.
72. Kadrmas DJ, Di Bella EVR, Khare HS, et al: Static versus dynamic teboroxime myocardial perfusion SPECT in canines. *IEEE Trans Nucl Sci* 47:1112–1117, 2000.
73. Bal H, Di Bella EVR, Gullberg GT: Parametric image formation using clustering for dynamic cardiac SPECT. *IEEE Trans Nucl Sci* 50:1584–1589, 2003.
74. Eberl S: *Quantitative Physiological Parameter Estimation from Dynamic Single Photon Emission Computed Tomography (SPECT).* PhD Thesis, Graduate School of Biomedical Engineering, The University of NSW, 2000.
75. Kuhl DE, Edwards RQ: Image separation radioisotope scanning. *Radiology* 80:653–661, 1963.
76. Stokely EM, Sveinsdottir E, Lassen NA, et al: A single photon dynamic computer assisted tomograph (DCAT) for imaging brain function in multiple cross sections. *J Comp Assis Tomogr* 4:230–240, 1980.
77. Kimura K, Hashikawa K, Etani H, et al: A new apparatus for brain imaging: Four-head rotating gamma camera single-photon emission computed tomograph. *J Nucl Med* 31:603–609, 1990.
78. Yonekura Y, Senda M, Fujita T, et al: System design and performance characteristics of newly developed whole-body multislice single photon emission computed tomography (abstract). *J Nucl Med* 26:P11, 1985.
79. Rowe RK, Barrett HH, Patton DD: The design and implementation of modular SPECT imaging systems. In Todd-Pokropek AE, Viergever MA (eds): *Medical Images: Formation, Handling, and Evaluation*, NATO-ASI Series. Heidelberg: Springer-Verlag, 1992.
80. Rogers WL, Clinthorne NH, Stramos JA, et al: SPRINT: A stationary detector single photon ring tomograph for brain imaging. *IEEE Trans Med Imag* MI-1:63–68, 1982.
81. Hirose Y, Ikeda Y, Higashi Y, et al: A hybrid emission CT Headtome II. *IEEE Trans Nucl Sci* NS-29:520–525, 1982.
82. Rogers WL, Clinthorne NH, Shao L, et al: SPRINT II: A second-generation single photon ring tomograph. *IEEE Trans Med Imag* MI-7:291–297, 1988.
83. Genna S, Smith AP: The development of ASPECT: An annular single brain camera for high efficiency SPECT. *IEEE Trans Nucl Sci* NS-35:654–658, 1988.
84. Rowe RK, Aarsvold JN, Barrett HH, et al: A stationary hemispherical SPECT imager for three-dimensional brain imaging. *J Nucl Med* 34:474–480, 1993.
85. Fick A: Sitzungsb. der Phys.-Med. Ges. zu Wurzburg, 1870, p. 36.
86. Stewart GN: Researches on the circulation time and on the influences which affect it: IV. The output of the heart. *J Physiol* 22:159–183, 1897.
87. Stewart GN: Researches on the circulation time and on the influences which affect it: V. The circulation time of the spleen, kidney, intestine, heart (coronary circulation) and retina, with some further observations on the time of the lesser circulation. *Am J Physiol* 58:278–295, 1921.
88. Hamilton WF, Moore JW, Kinsman JM, et al: Simultaneous determination of the pulmonary and systemic circulation times in man and of a figure related to the cardiac output. *Am J Physiol* 84:338–344, 1928.
89. Kety SS, Schmidt CF: The nitrous oxide method for the quantitative determination of cerebral blood flow in man: Theory, procedure, and normal values. *J Clin Invest* 27:476–483, 1948.
90. Meier P, Zierler KL: On the theory of the indicator-dilution method for measurement of blood flow and volume. *J Appl Physiol* 6:731–744, 1954.
91. Zierler KL: Equations for measuring blood flow by external monitoring of radioisotopes. *Circ Res* 16:309–321, 1965.
92. Lambrecht RM, Rescigno A: *Tracer Kinetics and Physiologic Modeling*. New York: Springer-Verlag, 1983.
93. Huang S-C, Phelps ME: Principles of tracer kinetic modeling in positron emission tomography and autoradiography. In Phelps ME, Mazziotta J, Schelbert H (eds): *Positron Emission Tomography and Autoradiography: Principles and Applications for the Brain and Heart*. New York: Raven Press, 1986, pp 287–346.
94. Bassingthwaighte JB, Raymond GM, Chan JI: Principles of tracer kinetics. In Zaret BL, Beller GA (eds): *Nuclear Cardiology: State of the Art and Future Directions*. St. Louis: Mosby, 1993, pp 3–23.
95. Rumsey WL, Rosenspine KC, Nunn AD: Myocardial extraction of teboroxime: Effects of teboroxime interaction with blood. *J Nucl Med* 33:94–101, 1992.
96. Gullberg GT, Huesman RH, Ross SG, et al: Dynamic cardiac single photon emission computed tomography. In Zaret BL, Beller GA (eds): *Nuclear Cardiology: State of the Art and Future Directions*. St. Louis: Mosby, 1999, pp 137–187.
97. Huesman RH, Knittel BL, Mazoyer BM, et al: Notes on RFIT: A program for fitting compartment models to region-of-interest dynamic emission tomography data. Lawrence Berkeley Laboratory Report no. LBL-37621, version 4.3, 1995.
98. Huesman RH, Mazoyer BM: Kinetic data analysis with a noisy input function. *Phys Med Biol* 32:1569–1579, 1987.
99. Lange K, Carson R: Reconstruction algorithms for emission and transmission tomography. *J Comput Assist Tomogr* 8:306–316, 1984.
100. Hudson HM, Larkin RS: Accelerated image reconstruction using ordered subsets of projection data. *IEEE Trans Med Imag* 13:601–609, 1994.
101. Levitan E, Herman GT: A maximum a posteriori probability expectation maximization algorithm for image reconstruction in emission tomography. *IEEE Trans Med Imag* MI-6:185–192, 1987.
102. Rao CR: *Linear Statistical Inference and Its Applications*. New York: Wiley, 1973.
103. Gullberg GT, Huesman RH, Ghosh Roy DN, et al: Estimation of the parameter covariance matrix for a one-compartment cardiac perfusion model estimated from a dynamic sequence reconstructed using MAP iterative reconstruction algorithms. In *2003 IEEE Nuclear Science Symposium and Medical Imaging Conference Record*, Oct. 19–25, 2003, Portland, Or.
104. Feng D, Huang SC, Wang X: Models for computer simulation studies of input functions for tracer kinetic modeling with positron emission tomography. *Int J Biomed Comput* 32:95–110, 1993.
105. Eberl S, Anayat AR, Fulton RR, et al: Evaluation of two population-based input functions for quantitative FDG PET studies. *Eur J Nucl Med* 24:299–304, 1997.
106. Deutsch R: *Estimation Theory*. Englewood Cliffs, NJ: Prentice-Hall, 1965.
107. Brownlee KA: *Statistical Theory and Methodology In Science and Engineering*, 2nd ed. Malabar, Fla: Robert E. Krieger Publishing, 1984.
108. Zar JH: *Biostatistical Analysis*, 2nd ed. Englewood Cliffs, NJ: Prentice-Hall, 1984.
109. Carson RE: Parameter estimation in positron emission tomography. In Phelps ME, Mazziotta J, Schelbert H (eds): *Positron Emission Tomography and Autoradiography: Principles and*

Applications for the Brain and Heart. New York: Raven Press, 1986, pp 347–390.
110. Sitek A, Gullberg GT, Huesman RH: Correction for ambiguous solutions in factor analysis using a penalized least squares objective. *IEEE Trans Med Imag* 21:216–225, 2002.
111. Sitek A, Gullberg GT, Di Bella EVR, et al: Reconstruction of dynamic renal tomographic data acquired by slow rotation. *J Nucl Med* 42:1704–1712, 2001.
112. Sitek A, Di Bella EVR, Gullberg GT, et al: Removal of liver activity contamination in teboroxime dynamic cardiac SPECT imaging using factor analysis. *J Nucl Cardiol* 9:197–205, 2002.
113. Wu H-M, Hoh CK, Choi Y, et al: Factor analysis for extraction of blood time-activity curves in dynamic FDG-PET studies. *J Nucl Med* 36:1714–1722, 1995.
114. Zaret BL: Pursuit of the ideal perfusion agent. *J Nucl Cardiol* 9:149–150, 2002.
115. McCulloch AD, Mazhari R: Regional myocardial mechanics: Integrative computational models of flow-function relations. *J Nucl Cardiol* 8:506–519, 2001.
116. L'Abbate A, Sambuceti G, Neglia D: Myocardial perfusion and coronary microcirculation: From pathophysiology to clinical application. *J Nucl Cardiol* 9:328–337, 2002.
117. Brown KA: Cardiac risk defined by stress myocardial perfusion imaging: Impact on physician decision making and cost savings. *J Nucl Cardiol* 9:124–126, 2002.
118. Heller GV: Acute rest myocardial perfusion imaging in the emergency department: A technique whose time has come . . . or gone? *J Nucl Cardiol* 9:350–352, 2002.
119. Angiolillo DJ, Giordano A: Role of myocardial perfusion imaging after coronary revascularization in symptom-free patients: Are low-risk patients really low? *J Nucl Cardiol* 9:550–553, 2002.
120. Brown KA: Prognostic value of myocardial perfusion imaging state-of-the-art and new developments. *J Nucl Cardiol* 3:516–537, 1996.
121. Elsasser A, Schlepper M, Klovekorn WP, et al: Hibernating myocardium, an incomplete adaptation to ischemia. *Circulation* 96:2920–2931, 1997.
122. Di Carli MF: Assessment of myocardial viability after myocardial infarction. *J Nucl Cardiol* 9:229–235, 2002.
123. Germano G, Kiat H, Kavanagh PB, et al: Automatic quantification of ejection fraction from gated myocardial perfusion SPECT. *J Nucl Med* 36:2138–2147, 1995.
124. Everaert H, Franken PR, Flamen P, et al: Left ventricular ejection fraction from gated SPET myocardial perfusion studies: A method based on the radial distribution of count rate density across the myocardial wall. *Eur J Nucl Med* 23:1628–1633, 1996.
125. Nakata T, Katagiri Y, Odawara Y, et al: Two- and three-dimensional assessment of myocardial perfusion and function by using technetium-99m sestamibi gated SPECT with a combination of count- and image-based techniques. *J Nucl Cardiol* 7:623–632, 2000.
126. Takeishi Y, Fujiwara S, Atsumi H, et al: Iodine-123-BMIPP imaging in unstable angina: A guide for interventional strategy. *J Nucl Med* 38:1407–1411, 1997.
127. Sandler MP, Patton JA: Fluorine 18-labeled fluorodeoxyglucose myocardial single-photon emission computed tomography: An alternative for determining myocardial viability. *J Nucl Cardiol* 3:342–349, 1996.
128. Delbeke D, Videlefsky S, Patton JA, et al: Rest myocardial perfusion/metabolism imaging using simultaneous dual-isotope acquisition SPECT with technetium-99m-MIBI/fluorine-18-FDG. *J Nucl Med* 36:2110–2119, 1995.
129. Di Carli MF, Maddahi J, Rokhsar S, et al: Long-term survival of patients with coronary artery disease and left ventricular dysfunction. Implications for the role of myocardial viability assessment I management decisions. *J Thorac Cardiovasc Surg* 116:997–1004, 1998.
130. Angeja BG, Gibson CM: Preserved coronary flow reserve in viable myocardium: Further evidence for the microvascular hypothesis. *Am Heart J* 141:329, 2001.
131. Gould KL, Lipscomb K: Effects of coronary stenoses on coronary flow reserve and resistance. *Am J Cardiol* 34:48–55, 1974.
132. Heller LI, Cates C, Popma J, et al: Intracoronary Doppler assessment of moderate coronary artery disease: Comparison with ^{201}Tl imaging and coronary angiography. FACTS Study Group. *Circulation* 96:484–490, 1997.
133. Marcus ML, Wilson RF, White CW: Methods of measurement of myocardial blood flow in patients: A critical review. *Circulation* 76:245–253, 1987.
134. Hoffman JI: Problems of coronary flow reserve. *Ann Biomed Eng* 28:884–896, 2000.
135. Strauer BE: The concept of coronary reserve. *J Cardiovasc Pharmacol* 19:S67–S80, 1992.
136. Doucette JW, Cori PD, Payne HM, et al: Validation of a Doppler guide wire for intravascular measurement of coronary artery flow velocity. *Circulation* 85:1899–1911, 1992.
137. Saraste M, Koskenvuo JW, Knuuti J, et al: Coronary flow reserve: measurement with transthoracic Doppler echocardiography is reproducible and comparable with positron emission tomography. *Clin Physiol* 21:114–122, 2001.
138. Schwitter J, Nanz D, Kneifel S, et al: Assessment of myocardial perfusion in coronary artery disease by magnetic resonance—A comparison with positron emission tomography and coronary angiography. *Circulation* 103:2230–2235, 2001.
139. Sugihara H, Yonekura Y, Kataoka K, et al: Estimation of coro-nary flow reserve with the use of dynamic planar and SPECT images of Tc-99m tetrofosmin. *J Nucl Cardiol* 8:575–579, 2001.
140. Leppo JA, DePuey EG, Johnson LL: A review of cardiac imaging with sestamibi and teboroxime. *J Nucl Med* 32:2012–2022, 1991.
141. Gray WA, Gewirtz H: Comparison of 99m-Tc-teboroxime with thallium for myocardial imaging in the presence of a coronary artery stenosis. *Circulation* 84:1796–1807, 1991.
142. Bontemps L, Geronicola-Trapali X, Sayegh Y, et al: Technetium-99m teboroxime scintigraphy. *Eur J Nucl Med* 18:732–739, 1991.
143. Drane WE, Keim S, Strickland P, et al: Preliminary report of SPECT imaging with Tc-99m teboroxime in ischemic heart disease. *Clin Nucl Med* 17:215–225, 1992.
144. Maublant JC, Marcaggi X, Lusson J-R, et al: Comparison between thallium-201 and technetium-99m methoxyisobutyl isonitrile defect size in single-photon emission computed tomography at rest, exercise and redistribution in coronary artery disease. *Am J Cardiol* 69:183–187, 1992.
145. Weinstein H, Dahlberg ST, McSherry BA, et al: Rapid redistribution of teboroxime. *Am J Card* 71:848–852, 1993.
146. Henzlova MJ, Machac J: Clinical utility of technetium-99m-teboroxime myocardial washout imaging. *J Nucl Med* 35:575–579, 1994.
147. Wu JC, Yun JJ, Dione DP, et al: Severe regional ischemia alters coronary flow reserve in the remote perfusion area. *J Nucl Cardiol* 7:43–52, 2000.
148. Rossen JD, Winniford MD: Effect of increases in heart rate and arterial pressure on coronary flow reserve in humans. *J Am Coll Cardiol* 21:343–348, 1993.
149. Ross SG, Gullberg GT, Huesman RH: The effect of heart motion on kinetic parameter estimates for dynamic cardiac SPECT. *IEEE Trans Nucl Sci* 44:1409–1416, 1997.
150. Di Bella EVR, Khare HS, Kadrmas DJ, et al: SPECT imaging of teboroxime during myocardial blood flow changes. *IEEE Trans Nucl Sci* 47:982–988, 2000.

151. Marshall RC, Powers-Risius P, Reutter BW, et al: Kinetic analysis of ^{125}I-iodorotenone as a deposited myocardial flow tracer: comparison with ^{99m}Tc-sestamibi. *J Nucl Med* 42:272–281, 2001.
152. Calnon DA, Ruiz M, Vanzetto G, et al: Myocardial uptake of (99m)Tc-N-NOET and (201)Tl during dobutamine infusion. Comparison with adenosine stress. *Circulation* 100:1653–1659, 1999.
153. Iida H, Itoh H, Bloomfield PM, et al: A method to quantitate cerebral blood flow using a rotating gamma camera and iodine-123 iodoamphetamine with one blood sampling. *Eur J Nucl Med* 21:1072–1084, 1994.
154. Gullberg GT: Kidney compartment model. Lawrence Berkeley Laboratory Report No. 2896, 1976.
155. Hansen L, Marzilli LG, Eshima D, et al: Evaluation of technetium-99m-triamide-mercaptide complexes designed to identify properties favoring renal tubular transport. *J Nucl Med* 35:1198–1205, 1994.
156. Coates C: Isotope lung imaging. *Curr Opin Radiol* 4:79–86, 1992.
157. Ercan MT, Ulutuncel N, Naldoken S: Evaluation of ^{99m}Tc-labelled alpha-D-glucose 1-phosphate aerosols for SPECT ventilation lung imaging. *Nucl Med Commun* 14:433–438,1993.
158. Gullberg GT, Ma X, Parker DL, et al: An MRI perfusion model incorporating nonequilibrium exchange between vascular and extravascular compartments. *Magn Reson Imag* 9:39–52, 1991.
159. Ma X, Gullberg GT, Parker DL: Magnetic resonance imaging verification of a multi-compartment perfusion model for a chromatography gel phantom. *Magn Reson Imag* 13:581–598, 1995.